Anti-viral responses of tissue-resident CD49a$^+$ lung NK cells are dysregulated in COPD

Grace E. Cooper[1]†, Jemma Mayall[2]†, Chantal Donovan[2,3], Tatt J. Haw[2], Kurtis F. Budden[2], Nicole G. Hansbro[3], Evy E. Blomme[4], Tania Maes[4], Chia Wei Kong[1], Jay C. Horvat[2], Salim I. Khakoo[1], Tom M.A. Wilkinson[1,5,6], Philip M. Hansbro[2,3]†*, Karl J. Staples[1,5,6]†*

[1] Clinical & Experimental Sciences, University of Southampton Faculty of Medicine, Sir Henry Wellcome Laboratories, Southampton General Hospital, Tremona Road, Southampton, SO16 6YD, UK.

[2] Priority Research Centre for Healthy Lungs, Hunter Medical Research Institute and University of Newcastle, Newcastle, NSW 2308, Australia.

[3] Centre for Inflammation, Centenary Institute and University of Technology Sydney, Faculty of Science, School of Life Sciences, Sydney, NSW 2007, Australia.

[4] Department of Respiratory Medicine, Laboratory for Translational Research in Obstructive Pulmonary Diseases, Ghent University Hospital, Ghent, Belgium.

[5] Southampton NIHR Respiratory Biomedical Research Unit, Southampton General Hospital, Southampton, UK.

[6] Wessex Investigational Sciences Hub, University of Southampton Faculty of Medicine, Southampton General Hospital, Southampton, UK.

† These authors contributed equally to this work

*Corresponding authors: Karl J Staples (k.staples@southampton.ac.uk) and Philip Hansbro (Philip.Hansbro@uts.edu.au)

Tissue-resident lung NK cells are differentially affected by COPD development compared to circulating NK cells in both mice and humans and this may contribute to excess inflammation in viral exacerbations of COPD. Understanding the function of lung-resident innate immune cells during COPD development and exacerbation is important to our overall understanding of immune dysregulation in this disease and for potential therapeutic intervention.

Author Contributions: Study conceptualization by GC, JM, TW, KS, PH, investigation by GC, JM, EB, CK methodology by GC, JM, CD, KB, EB, TH, NH, JH, SK and funding acquisition by TM, TW, PH, KS. Original manuscript drafting by GC and JM, all authors contributed to manuscript review and editing.

Sources of Support: This work was part funded by the BMA HC Roscoe Award 2013 to KS and TW and a 4-year MRC PhD studentship. We also gratefully acknowledge the support of the European Respiratory Society Short Term Research Fellowship 2017 and the support of the Southampton AAIR charity in funding this work. The murine studies were funded by fellowships and grants from the National Health and Medical Research Council (NHMRC) of Australia (1079187, 1099095, 1138004, 1137995, 1175134) to PMH and FWO Flanders (G053516N) to TM and EB.

Running Head: Tissue-resident NK cells in COPD

Descriptor Number: 7.18 Mucosal Immunity of the Respiratory Tract

Word Count: 4011

This article has an online data supplement, which is accessible from this issue's table of content online at www.atsjournals.org.

Abstract

Rationale: Tissue-resident natural killer cells have been identified in numerous organs, but little is known about their functional contribution to respiratory immunity, in particular during chronic lung diseases such as COPD.

Objectives: To investigate the phenotype and antiviral responses of trNK cells in murine cigarette smoke-induced experimental COPD and in human lung parenchyma from COPD donors.

Methods: Mice were exposed to cigarette smoke for 10 weeks to induce COPD-like lung disease. Lung tissue resident NK cell phenotypes and function were analysed by flow cytometry in both murine and human disease with and without challenge with influenza A virus.

Measurements and Main Results: In the mouse lung $CD49a^{+}CD49b^{+}EOMES^{+}$ and $CD49a^{+}CD49b^{-}EOMES^{lo}$ NK cell populations had a distinct phenotype compared with CD49a- circulating NK cells. $CD49a^{+}$ NK cells were more extensively altered earlier in disease onset than circulating NK cells and increased proportions of CD49a+ NK cells correlated with worsening disease in both murine and human COPD. Furthermore, the presence of lung disease delayed both circulating and tissue-resident NK cell functional responses to influenza infection. CD49a+ NK cells markedly increased their NKG2D, CD103 and CD69 expression in experimental COPD following influenza infection, and human CD49a+ NK cells were hyperactive to *ex vivo* influenza infection in COPD donors.

Conclusions: Collectively, these results demonstrate that tissue-resident NK cell function is altered in cigarette smoke-induced disease and suggests that smoke exposure may aberrantly prime tissue-resident NK cell responsiveness to viral infection. This may contribute to excess inflammation during viral exacerbations of COPD.

Abstract word count: 246

Immunity, Innate

Immunity, Mucosal

Pulmonary Disease, Chronic Obstructive

Influenza, Human

INTRODUCTION

Chronic obstructive pulmonary disease (COPD) is a chronic inflammatory condition of the lungs and is the third leading cause of death globally [1,2]. Seasonal viruses, including Influenza A Virus (IAV) are identified in >30% of COPD exacerbations and are a major driver of mortality and morbidity[3–5]. Immune dysregulation in COPD is well characterised, with chronic inflammation and poor function of both innate and adaptive immunity, including NK cells [6,7]. NK cells have important roles in immunity through their cytotoxic effector function and inflammatory cytokine release[8]. Found in high abundance in the blood, spleen and lungs, murine NK cell developmental stage is commonly distinguished through CD11b and CD27 expression[9]. In humans, immature and mature NK cells are commonly reported as $CD56^{bright}$ and $CD56^{dim}$ respectively, with $CD56^{bright}CD16^{-}$ NK cells poorly cytotoxic but potent cytokine producers[8].

NK cells from COPD-affected lung tissue have enhanced killing of respiratory epithelia and are linked to an emphysematous phenotypes in cigarette smoke (CS)-exposed mice, suggesting that overactive NK cells may contribute to tissue destruction in COPD [6,7,10–12]. There is an emerging role for NK cells in COPD exacerbations, given their roles in responding to IAV[13–21]. In fact Osterburg *et al.* (2020) demonstrated distinct and stable changes in peripheral blood NK cells following COPD exacerbation [22]. Phenotypically unique subsets of NK cells have been identified in the lung and are likely tissue-resident, based on a transcriptional signature similar to resident memory T cells and integrin expression such as CD69, CD49a (integrin α2) and CD103 (integrin αE) [20,23–25]. CD49a is commonly reported as a dominant marker of lung trNK cell phenotype, with ~13% of human lung NK cells expressing this integrin [20,24]. Although the functional importance of lung trNK cells remains to be fully explored, early work suggested that lung trNK

cells are hyper-reactive to IAV infection, ultimately becoming the dominant polyfunctional NK cell population in *ex vivo* lung infection [20,25].

Thus far, studies investigating the relationship between NK cell function and COPD have not discriminated between circulating NK (cNK) and lung trNK cells. Indeed, the contribution of trNK cells during COPD pathogenesis and exacerbation is unknown. To define the antiviral responses of lung trNK cells in COPD, the phenotype and function of trNK cells were analysed during the onset and development of CS-induced experimental COPD, *in vivo* IAV-induced exacerbation and *ex vivo* IAV infection of human COPD lung tissue.

MATERIALS AND METHODS

Murine models. Female C57BL/6 mice were exposed to the smoke from 12 3R4F cigarettes, twice a day, 5 times a week for up to 12 weeks, as described previously[26–31]. 3R4F contain 11.0mg particulate matter/cig that is predominantly PM_{10} and $PM_{2.5}$ [32]. Some groups were intranasally inoculated with IAV (A/PR/8/34 mouse-adapted H1N1, 33 plaque forming units, in 50μL UltraMDCK media) under isoflurane anaesthesia [33–35]. This model of CS-induced COPD recapitulated the features of human disease, including emphysema-like alveolar enlargement (Fig. E1). Mice were euthanized by sodium pentobarbital (Lethabarb; Virbac) overdose at the endpoint. Experiments were approved by the University of Newcastle Animal Care and Ethics Committee and performed at the Hunter Medical Research Institute, NSW, Australia.

Murine immune cell isolation and analysis. Lungs were digested with collagenase D (Roche), processed into single cell suspensions and stimulated with Phorbol 12-myristate 13-acetate and Ionomycin (PMA/I) with brefeldin A (Sigma) before cells were stained and analyzed by flow cytometry as described in the online supplement.

Emphysema. Lung tissue was formalin fixed, sectioned and stained and emphysema-like alveolar enlargement quantified using the MLI technique, as previously described and as in the online supplement [28–31].

Human tissue donor recruitment and sample collection. Human lung tissue and blood was collected from donors undergoing cancer resection surgeries taking place at Southampton General Hospital (approved by Southampton and South West Hampshire Research Ethics Committee, UK

09/H0504/109), and all participants provided informed written consent. Lung tissue was obtained from sites distal to tumours that were reported as macroscopically normal. Donors were divided into COPD and non-COPD groups retrospectively via assessment of medical records, spirometry and lung imaging. A comprehensive description of donor demographics is included in the online supplement.

Analysis of human lung tissue and explant infection. Lung tissue explants were prepared and infected with IAV (X31 H3N2, Virapur) before infected and uninfected tissue was digested into single cells suspensions and stained for flow cytometry as described previously and as in the online supplement[36–38].

Statistical analyses. Data are presented as individual values with mean or median summarized, as indicated. Comparisons between two groups were performed using an unpaired two-tailed t-test or or Mann-Whitney test, as appropriate. Comparisons involving three or more groups were performed by one-way ANOVA with Bonferroni's multiple comparison correction post-hoc test. Comparisons between different cell populations within the same subject were performed using appropriate grouped analyses (paired t-test, Wilcoxon signed-rank test or repeated measures one-way ANOVA with Bonferroni's post-hoc test), as indicated. Groups of CS-treated mice were compared against matched air-controls analysed at the same time. Pearson correlation co-efficient and P value and simple linear regression were calculated for correlations between NK cell population frequencies and FEV_1%. Statistical analyses were performed using GraphPad Prism 9 software (San Diego, CA).

RESULTS

Murine lung CD49a$^+$ NK cells have a distinct phenotype

Three sub-populations of NK cells were identified in the naïve murine lung, CD49a$^-$CD49b^{var} cNK cells, putative CD49a$^+$CD49b$^-$ trNK cells, and CD49a$^+$CD49b$^+$ trNK cells, with the majority being CD49a$^-$CD49b^{var} cNK cells (90.1%±7.9) (Fig. 1A-C). CD49a$^+$CD49b$^+$ and CD49a$^+$CD49b$^-$ NK populations had greater expression of the activating receptor, NKG2D, and CD103 compared to CD49a$^-$CD49b$^+$ cNK cells (Fig. 1D, E). All NK cell subsets expressed higher levels of EOMES compared to CD3$^+$NK1.1$^-$ T cells (Fig. 1F), with CD49a$^+$CD49b$^+$ expressing higher, and CD49a$^+$CD49b$^-$ NK cells expressing less, compared to CD49a$^-$CD49b^{var} NK cells. Both CD49a$^+$CD49b$^-$ and CD49a$^+$CD49b$^+$ NK cell subsets upregulated granzyme-B following PMA/I stimulation, indicating potential cytotoxic function (Fig. 1G). Therefore, both subsets of CD3$^-$ NK1.1$^+$CD49a$^+$ cells are EOMES$^+$ and granzyme-B$^+$ indicating they are trNK, rather than ILC1[19,39–43].

Most murine lung NK cells were mature (CD27$^-$CD11b$^+$) cytotoxic effectors, with small populations of immature and differentiating NK cells (CD27$^{+/-}$ CD11b$^-$) identified (Fig. E2 B-D). Approximately 20% of CD11b$^-$ cells were CD49a$^+$, whilst around 5% of CD11b$^+$ NK cells were CD49a$^+$ (Fig. 1 H and I). This expression of CD49a on immature NK cells fits with descriptions of CD49a$^+$ lung NK cells in humans and indicates consistency between human and mouse trNK cell biology[19,20].

The development and progression of experimental COPD is associated with altered lung NK cell numbers

Lung NK cell populations were next assessed in air- or CS-exposed mice after 1 week (acute CS exposure), 8 weeks (emergence of chronic disease features) or 12 weeks (progressive and fully irreversible disease)[26–31]. Experiments at these points of disease were performed independently and are analysed as such, CS-treated mice are compared against matched air controls in the same experiment. This widely used mouse model of CS-induced experimental COPD recapitulates the characteristic clinical features of human COPD by 8 weeks, including inflammation, airway remodeling, mucus hypersecretion, emphysema-like alveolar destruction, impaired lung function and non-responsiveness to corticosteroid treatment[26–31]. At 12 weeks, CS-exposed mice exhibit substantial lung disease with chronic airway inflammation, airway fibrosis, and an irreversible decline in lung function.

We show that the proportion of NK cells (defined as $CD45^+CD3^-NK1.1^+$ cells) decreased (20.3% to 9.9% of lung $CD45^+$ lymphocytes) following 12 weeks of CS exposure (FigE2 E,F). Following 1 week of CS exposure $CD49a^+CD49b^-$ trNK cell numbers increased, whilst $CD49a^-$ and $CD49a^+CD49b^+$ numbers remained unchanged (Fig. 2A-C). However, the number of cNK cells ($CD49a^-CD49b^{var}$) was reduced following 8 weeks and trended towards reduction at 12 weeks of CS exposure (Fig. 2A). The numbers of $CD49a^+CD49b^-$ and $CD49a^+CD49b^+$NK cells were both reduced (-47% and -31%, respectively) after 12 weeks of exposure (Fig. 2B,C). A reduction in $CD49a^+CD49b^+$ cells was also observed at 8 weeks of CS exposure. These results show that $CD49a^+CD49b^-$ cells are increased early during CS-induced inflammation while both $CD49a^+$ and $CD49a^-$ NK cell subsets are reduced in the lungs of mice later during CS-induced experimental COPD.

trNK cell functional markers are disproportionally affected by CS exposure

Surface CD69 (Fig. 3A) and intracellular IFN-γ (Fig. 3B) expression upon PMA/I stimulation were unchanged in all subsets of NK cells following 1 week of CS exposure. However, CD69 expression was increased on $CD49a^{+}CD49b^{-}$ and $CD49a^{+}CD49b^{+}$ NK cells (Fig. 3A), and IFN-γ production reduced in $CD49a^{+}CD49b^{-}$ NK cells (Fig. 3B) following 8 and 12 weeks of CS exposure. cNK only showed increased CD69 following 12 weeks of CS exposure. At steady state, $CD49a^{+}CD49b^{-}$ NK cells expressed the highest frequency of CD69, fitting with its involvement in tissue retention (Fig. 3A). CS-induced COPD was associated with dramatically increased CD103 expression on all lung NK cell subsets, with the greatest increase on $CD49a^{+}CD49b^{+}$ NK cells after 12 weeks (Fig. 3C). The effects of CS exposure on lung NK cell phenotype can also be appreciated as fold change in protein expression as shown in Fig. E4. These results demonstrate altered phenotypes of both cNK ($CD49a^{-}$) and trNK ($CD49a^{+}$) cells during CS-induced experimental COPD, with the most marked changes observed in trNK cells. Importantly, trNK cell phenotype is altered earlier during CS-induced COPD than cNK cells.

Chronic CS exposure impairs cNK and trNK cell responses to IAV infection

We next exposed mice to air or CS for 10 weeks prior to infecting them with IAV to determine how experimental COPD affects NK responses to IAV infection early during the innate phase (3 days post-inoculation [dpi]) and at the peak of infection [7dpi]) (Fig. 4 and E3) [34,35]. $CD49a^{-}CD49b^{var}$ and $CD49a^{+}CD49b^{+}$, but not $CD49a^{+}CD49b^{-}$, NK cell subsets were increased at 3dpi in air-exposed mice infected with IAV (Fig. 4A-C). There were no differences in air-exposed mice by 7dpi (Fig. 4D and E). Significantly, CS exposure suppressed NK cell numbers in the lungs of IAV-infected mice at 3dpi compared to controls (Fig. 4A-C). Interestingly, all three NK cell

populations were increased at 7dpi in IAV-infected, CS-exposed mice (Fig. 4D-F) compared to sham-infected, CS-exposed and IAV-infected, air-exposed controls. These findings show that NK cell responses to IAV are delayed in experimental COPD.

cNK and trNK cell functional markers during IAV infection are dysregulated by experimental COPD

We show that IAV infection increases IFN-γ production in all three NK cell subsets in air-exposed mice (3 dpi) and this IFN-γ response to IAV in cNK and $CD49a^{+}CD49b^{+}$ trNK cells is unchanged in CS-exposed mice compared to air-exposed controls (Fig. 5A). Interestingly, we show that IFN-γ production by $CD49a^{+}CD49b^{-}$ NK cells in response to IAV was completely abrogated in CS-exposed mice compared to air-exposed controls (Fig. 5A). Increased expression of the marker of degranulation, CD107a, in air-exposed mice in response to IAV infection only occurred in $CD49a^{+}CD49b^{-}$ NK cells at 3dpi (Fig. 5B). CD107a expression was not altered on $CD49a^{+}CD49b^{+}$ NK cells, but was suppressed on $CD49a^{+}CD49b^{-}$ NK cells in CS-exposed mice, indicating that experimental COPD may abrogate $CD49a^{+}CD49b^{-}$ NK cytotoxic capacity. Furthermore, CS exposure increased CD107a expression on $CD49a^{-}CD49b^{var}$ cNK cells in sham-infected mice compared to air-exposed, sham-infected controls and this was further enhanced in CS-exposed, IAV-infected mice (Fig. 5B), indicating enhanced cytotoxic responses of cNK cells in CS-induced experimental COPD. NKG2D, an activating receptor important in the recognition and destruction of IAV-infected cells and NK cell-mediated epithelial cell destruction in COPD, was increased on all NK cell subsets following IAV infection in both air- and CS-exposed mice (Fig. 5C), with greater expression seen in CS-exposed mice compared to air-exposed controls. Interestingly, experimental COPD enhanced NKG2D expression on trNK cell subsets but not cNK cells, in the

absence of IAV infection. CD69 frequency was also increased on all NK cell subsets following IAV infection and this was further increased in CS-exposed groups (Fig. 5D). Interestingly, trNK cell subsets had the greatest increase in NKG2D and CD69 expression in IAV-infected, CS-exposed mice. CD103 expression was not affected by IAV infection in either air- or CS-exposed mice (Fig. 5E). Collectively these data indicate a dysregulated anti-viral NK cell response in experimental COPD. Similar findings were observed following IAV infection at 7dpi (Fig. E6), with the exception of NKG2D.

CD49a^{+} NK cell numbers correlate with more severe disease in patients with COPD

We next investigated the relationship between lung trNK cell subset frequency and human COPD. Human NK cells, which lack expression of CD49b, were identified in lung parenchyma as CD3^{-} CD56^{+} cells and further defined as CD56^{bright}, CD56^{dim}CD16^{+} and CD56^{dim}CD16^{-} subsets and their expression of CD49a assessed (Fig. E7) [20]. The greatest frequency of CD49a expression was observed on immature CD56^{bright} NK cells, followed by lower levels on CD56^{dim}CD16^{-} NK cells, with negligible expression detected on mature CD56^{dim}CD16^{+} subsets (Fig. E7).

There was no correlation between the proportion of CD45^{+} lung lymphocytes identified as NK cells and FEV_1% predicted in a mixed cohort of subjects with and without COPD (Fig. 6A). However, an increased proportion of CD56^{bright} NK cells correlated with reduced FEV_1 % predicted (Fig. 6B), while an increase in CD56^{dim}CD16^{+} NK cell frequency correlated with increased FEV_1 % predicted (Fig. 6C). Importantly, the frequency of CD49a on CD56^{bright} NK cells negatively correlated with donor FEV_1 % predicted, with higher proportions of CD49a^{+} NK cells observed in subjects with more severe disease (Fig. 6E and Fig. E8A and B). No relationship

was observed between $CD56^{dim}CD16^{-}$ NK cells and lung function (Fig. 6D) or with CD49a expression in this subset (Fig. 6F). The proportions of all NK cell subsets, including trNK cells, were unaffected by inhaled corticosteroid use or smoking status (Fig. E8 C-L). Pack year history (where it was known) was not found to correlate with FEV1% (Fig. 6G), which most likely reflects a strong history of smoking in the non-COPD, cancer resection cohort.

Importantly, we show that equivalent shifts in NK cell phenotype occur in mice during experimental COPD, with the proportion of $CD11b^{-}$ NK cells (Fig. 6H; as a proportion of $CD3^{-}$ $NK1.1^{+}$ NK cells) and the frequency of CD49a expression on these $CD11b^{-}$ populations (Fig. 6I) increasing in the lungs of CS-exposed mice compared to air-exposed controls. These results indicate that NK cell numbers and phenotype are altered in COPD, with a skew towards more immature NK cells and a higher frequency of $CD49a^{+}CD56^{bright}/CD11b^{-}$ trNK cells with disease.

$CD49a^{+}$ NK cells in the human lung are phenotypically distinct from $CD49a^{-}$ NK cells

We next analysed the expression of NK cell activating receptors NKp46, NKG2D, NKG2C and the chemokine receptor CCR5 on CD49a+ and CD49a- cells in lung single cells from subjects with and without COPD. $CD49a^{+}CD56^{bright}$ NK cells expressed lower levels of NKp46 (P=0.04), but higher levels of NKG2D (P=0.0039), NKG2C (P=0.0049) and CCR5 (P=0.0039) than $CD49a^{-}$ $CD56^{bright}$ NK cells (Fig. 7 A-E). However, CCR5 expression was greater on all subsets of NK cells analysed from the lung, compared with those isolated from matched donor blood, implicating this chemokine receptor in general NK cell homing to the lung (Fig. E9A and B). CD49a was also expressed by $CD56^{dim}CD16^{-}$ cells (Fig. E7) and interestingly, similar trends were observed in the phenotype of these cells, with $CD49a^{+}CD56^{dim}CD16^{-}$ cells also expressing more NKG2D and

CCR5 (P=0.042 and 0.0078 respectively, Fig. E9C and F). Although $CD49a^+$ trNK cells had a distinct phenotype compared with circulating $CD49a^-$ NK cells in the lungs, the COPD status of the donor did not affect $CD49a^+$ phenotype in our study (Fig. E10). Taken together this data indicates that there is a distinct phenotype of $CD49a^+$ human lung NK cells compared with $CD49a^-$ NK cells, that is not explained by COPD status.

$CD49a^+$ NK cells in the COPD lung are more responsive to IAV infection than $CD49a^-$ NK cells

To better understand the functional potential of human lung trNK cells in COPD, human lung tissue was infected *ex vivo* with IAV (X31 H3N2) and NK cell production IFN-γ production was assessed. NK cells from COPD lungs produced IFN-γ, whilst no IFN-γ was detected in NK cells from non-COPD lungs (P=0.0079, Fig. 7F and J). Analysis of NK cell subsets in IAV-infected lungs showed that IFN-γ production was primarily detected in $CD56^{bright}CD16^-$ (P=0.032) and $CD56^{dim}CD16^-$ (P=0.019) NK cells, with less prominent IFN-γ upregulation in $CD56^{dim}CD16^+$ cells (P=0.086) (Fig. 7 G-I). Furthermore, $CD49a^+$ cells in both $CD56^{bright}$ and $CD56^{dim}$ subsets were the major producers of driving IFN-γ production in COPD tissue (P=0.071 and P=0.012, Fig. 7K and L). This data suggests that trNK cells may be hyper-responsive to IAV in the human COPD lung.

DISCUSSION

In this study we progress the current understanding of immune dysfunction in COPD by providing evidence of cNK and trNK cell dysregulation in both human and experimental COPD. In the mouse the majority of lung NK cells were circulating ($CD49a^-$) with small proportions of $CD49a^+$ trNK cells (9%, Fig. 1B), similar to that found in humans (13%)[20]. In both murine and human lung tissue CD49a was expressed on predominantly immature NK cell subsets ($CD11b^-$ in mice and $CD56^{bright}$ in humans) with little to no expression on differentiated cytotoxic effectors (Fig. E7 and Fig. 1H and I)[20]. $CD49a^+$ trNK cell populations had distinct phenotypes in both species, with increased NKG2D, CD103 and CD69 relative to cNK cells. Furthermore, a switch to a higher proportion of $CD49a^+$ immature NK cells in the lungs correlated with human disease (Figure 6E) and development of COPD in a murine model (Figure 3). Together, these data show that both tr and cNK cells are dysregulated in CS-induced disease and that there is a high parity between lung trNK cell biology in experimental and human COPD.

Heightened NK cell cytotoxicity and destruction of autologous epithelial cells has previously been described in COPD and is driven through enhanced dendritic cell signalling[6,7]. Our data is concurrent with this as we have also described evidence of degranulation (enhanced surface CD107a) on cNK cells and we add to this understanding by demonstrating a further enhancement of the degranulation response to IAV infection after CS exposure. However, until now, studies investigating NK cell function in COPD have only considered cNK cells. For instance, we observe upregulation of NKG2D (an activating receptor associated with enhanced NK cell cytotoxicity in COPD) on the cNK pool as described previously[44,45]. NKG2D ligands are upregulated on structural cells of COPD airways and may be a key driver of NK cell activation. However, larger

increases in NKG2D expression were identified on CD49a+ trNK cell subsets, which is concurrent with increases in other markers of residency and activation, such as CD69 and CD103, in these populations.

In our model of experimental COPD we investigated trNK cell phenotypes at three distinct points in disease development. trNK cell phenotypes were altered earlier than cNK cells, with increased CD69 and CD103 on $CD49a^+$ NK cells at 8 weeks of CS exposure (at disease onset) whereas these increases were only observed on cNK cells at 12 weeks of CS exposure (progressive disease). Interestingly, CD69 and CD103 are classic tissue residency markers and their upregulation following CS exposure may indicate a drive towards greater residency in diseased lung tissue.

IAV has an important role in driving disease exacerbations in human COPD[34,35,46]. In air-exposed control mice a strong NK cell functional response was identified 3dpi, with population expansions of cNK and $CD49a^+CD49b^+$ NK cells, IFN-γ production and increased NKG2D and CD69 surface expression in all subsets (Fig 5). However, CD107a was only identified on $CD49a^+CD49b^-$ NK cells post IAV infection in air controls. In CS-exposed mice, expansion of cNK was delayed to 7dpi, with $CD49a^+CD49b^-$ NK cells also increased (Fig. 4). In addition, CS exposure enhanced post-IAV degranulation of cNK cells and increased NKG2D, CD69 and CD103 expression on cNK and trNK subsets, with $CD49a^+$ trNK cells demonstrating the greatest increases in all three markers. This distortion in the NK cell response and particularly the delay in NK cell expansion, may contribute to the exacerbation of COPD during viral infection and lack of viral clearance[34,35,47–50]. We propose that changes in trNK cell populations indicate a potentially

aberrant priming of response to IAV infection and a CS-induced shift from a protective NK cell response to one that may contribute to excessive inflammation and tissue damage.

CD49a^{+}CD49b^{-} NK cells express higher NKG2D but lower EOMES, Gzm-B and CD107a relative to CD49a^{+}CD4b^{+} lung NK cells, but only CD49a^{+}CD49b^{-} NK cells provided evidence of degranulation in response to IAV. These differences might reflect a greater cytotoxic capacity in CD49a^{+}CD49b^{-} NK cells or point towards other different functional responses in the two populations. However, heterogeneity of CD49b expression within the CD49a+ population may simply enable residency in different parts of the lung tissue due to different collagen/laminin specificities and may not impact function, however this remains to be explored directly.

Although the IFN-γ response of trNK cells was unchanged or diminished in experimental COPD, in *ex vivo* infection of human lung tissue explants NK cell IFN-γ production was only identified in CD49a^{+} lung trNK cells from COPD donors (Figure 7). This suggests a hyper-responsiveness of CD49a^{+} NK cells to IAV in human COPD and a potential link to exacerbation of underlying disease. This apparent species difference may reflect a life-time exposure to IAV in human donors, versus novel pathogen exposure in the mouse. However, it is interesting that in experimental COPD an altered trNK cell phenotype is observed with enhanced markers of activation (CD69/NKG2D) and residency (CD103). Human CD49a^{+} lung NK cells express more NKG2D (Fig 7B) which may explain the heightened response of CD49a^{+} NK cells to IAV[19–21]. If trNK cells are primed through NKG2D signaling in COPD tissue, this may drive the observed IFN-γ production from these cells during *ex vivo* infection.

Due to logistical constraints on cage number, the smoking experiments described here were only performed with female mice, limiting the applicability of this data for the male gender. Furthermore, our analysis of CS effect over time of smoke exposure was designed as three independent experiments and should be considered as such, rather than a true timecourse and recognize the use of single animal experiments as a limitation. In addition, it should be noted that all human lung tissue was obtained from cancer resection surgeries and the effect of lung tumour on the NK cell phenotype cannot be fully excluded from our analysis. However, in line with our previous work using resected human lung tissue, we have still observed COPD-related effects on immune cell function over and above the presence of cancer[36]. We recognize the small number of human samples analyzed as a limitation and that these data only provide insight into mild-moderate COPD rather than more severe disease. In addition, there are also significant differences in NK cell marker expression between mice and humans that limit our ability to draw a direct link between the populations described here, most notably a lack of NK1.1 and CD49b in humans and CD56 in mice. Lastly, IAV infection in the murine model represents the introduction of novel pathogen whereas *ex vivo* IAV infection of human lung tissue is more likely to be recognized by existing arms of the immune system due to the high circulation of this virus and age of the tissue donors. Therefore, some of the species differences observed in this study may reflect this underlying difference in immune-biology of novel vs recurring infection.

Overall, this work demonstrates the complex effects of smoking and inflammatory disease on the phenotype and function of lung-resident NK cells and provides evidence of trNK cell dysregulation in murine and human COPD. In the murine model of experimental COPD trNK cells demonstrate large increases in the expression of CD69 and NKG2D following IAV infection, with suppression

of IFN-γ and CD107a. In human COPD, an *ex vivo* IAV infection of lung tissue elicits fast IFN-γ production from trNK cells, indicating a potentially aberrant and detrimental response to IAV that may contribute to excess inflammation and exacerbation of disease. trNK cells express integrins that bind collagen IV and E-cadherin (CD49a and CD103, respectively) and therefore may be located close to the epithelial layer of the lungs. Given the potential of these cells to respond to local insults and mediate heightened inflammatory responses, understanding this dysregulated innate immunity in COPD is important to intervening during disease development and exacerbation.

Acknowledgments: The authors wish to thank Richard Jewell and Dr Carolann MacGuire of the University of Southampton, Faculty of Medicine Flow Cytometry Unit and the University of Newcastle Analytical and Biomolecular Research Facility. We thank the staff and students of the Hansbro lab who helped run the labor-intensive murine CS exposure models, Bradley Mitchell, Bre Anderson, Dr Kurtis Budden, Dr Henry Gomez, Dr Priyanka Sahu, Dr Lohis Balachandran, Sophie Pickles, Saima Firdous Rehman, Dr Vrushali Chimankar, Xiaofan Tu, and Vinod Kumar. We also express our appreciation to Christian Ottensmeier, Benjamin Johnson, Carine Fixmer and the rest of the Target Lung staff who co-ordinated human lung tissue samples. We extend our gratitude to all the volunteers who provided lung and blood samples.

References

1. Vestbo, J., Hurd, S. S., Agustí, A. G., Jones, P. W., Vogelmeier, C., Anzueto, A., *et al.* Global strategy for the diagnosis, management, and prevention of chronic obstructive pulmonary disease GOLD executive summary. *American Journal of Respiratory and Critical Care Medicine* vol. 187 347–365 (2013).
2. Barnes, P. J. Inflammatory mechanisms in patients with chronic obstructive pulmonary disease. *J Allergy Clin Immunol* **138**, 16–27 (2016).
3. Barnes, P. J., Burney, P. G. J., Silverman, E. K., Celli, B. R., Vestbo, J., Wedzicha, J. A., *et al.* Chronic obstructive pulmonary disease. *Nature Reviews Disease Primers* **1**, 1–21 (2015).
4. Bekkat-Berkani, R., Wilkinson, T., Buchy, P., dos Santos, G., Stefanidis, D., Devaster, J.-M., *et al.* Seasonal influenza vaccination in patients with COPD: a systematic literature review. *BMC Pulm Med* **17**, 79 (2017).
5. Sethi, S. Infection as a comorbidity of COPD. *European Respiratory Journal* **35**, 1209–1215 (2010).
6. Finch, D. K., Stolberg, V. R., Ferguson, J., Alikaj, H., Kady, M. R., Richmond, B. W., *et al.* Lung Dendritic Cells Drive NK Cytotoxicity in Chronic Obstructive Pulmonary Disease via IL-15Ralpha. *Am J Respir Crit Care Med* (2018) doi:10.1164/rccm.201712-2513OC.
7. Freeman, C. M., Stolberg, V. R., Crudgington, S., Martinez, F. J., Han, M. K., Chensue, S. W., *et al.* Human CD56+ cytotoxic lung lymphocytes kill autologous lung cells in chronic obstructive pulmonary disease. *PLoS One* **9**, e103840 (2014).

8. Abel, A. M., Yang, C., Thakar, M. S. & Malarkannan, S. Natural killer cells: Development, maturation, and clinical utilization. *Frontiers in Immunology* vol. 9 1869 (2018).
9. Goh, W. & Huntington, N. D. Regulation of Murine Natural Killer Cell Development . *Frontiers in Immunology* vol. 8 130 (2017).
10. Motz, G. T., Eppert, B. L., Wortham, B. W., Amos-Kroohs, R. M., Flury, J. L., Wesselkamper, S. C., *et al.* Chronic Cigarette Smoke Exposure Primes NK Cell Activation in a Mouse Model of Chronic Obstructive Pulmonary Disease. *The Journal of Immunology* **184**, 4460–4469 (2010).
11. Wortham, B. W., Eppert, B. L., Flury, J. L., Morgado Garcia, S. & Borchers, M. T. TLR and NKG2D signaling pathways mediate CS-induced pulmonary pathologies. *PLoS One* **8**, e78735 (2013).
12. Stolberg, V. R., Martin, B., Mancuso, P., Olszewski, M. A., Freeman, C. M., Curtis, J. L., *et al.* Role of CC chemokine receptor 4 in natural killer cell activation during acute cigarette smoke exposure. *Am J Pathol* **184**, 454–463 (2014).
13. Stein-Streilein, J. & Guffee, J. In vivo treatment of mice and hamsters with antibodies to asialo GM1 increases morbidity and mortality to pulmonary influenza infection. *J Immunol* **136**, 1435–1441 (1986).
14. Gazit, R., Gruda, R., Elboim, M., Arnon, T. I., Katz, G., Achdout, H., *et al.* Lethal influenza infection in the absence of the natural killer cell receptor gene Ncr1. *Nat Immunol* **7**, 517–523 (2006).

15. Nogusa, S., Ritz, B. W., Kassim, S. H., Jennings, S. R. & Gardner, E. M. Characterization of age-related changes in natural killer cells during primary influenza infection in mice. *Mech Ageing Dev* **129**, 223–230 (2008).

16. Zhou, K., Wang, J., Li, A., Zhao, W., Wang, D., Zhang, W., *et al.* Swift and Strong NK Cell Responses Protect 129 Mice against High-Dose Influenza Virus Infection. *J Immunol* **196**, 1842–1854 (2016).

17. Abdul-Careem, M. F., Mian, M. F., Yue, G., Gillgrass, A., Chenoweth, M. J., Barra, N. G., *et al.* Critical role of natural killer cells in lung immunopathology during influenza infection in mice. *J Infect Dis* **206**, 167–177 (2012).

18. Zhou, G., Juang, S. W. & Kane, K. P. NK cells exacerbate the pathology of influenza virus infection in mice. *Eur J Immunol* **43**, 929–938 (2013).

19. Scharenberg, M., Vangeti, S., Kekäläinen, E., Bergman, P., Al-Ameri, M., Johansson, N., *et al.* Influenza A Virus Infection Induces Hyperresponsiveness in Human Lung Tissue-Resident and Peripheral Blood NK Cells. *Frontiers in Immunology* **10**, 1116 (2019).

20. Cooper, G. E., Ostridge, K., Khakoo, S. I., Wilkinson, T. M. A. & Staples, K. J. Human CD49a+ lung natural killer cell cytotoxicity in response to influenza A virus. *Frontiers in Immunology* **9**, 1671 (2018).

21. Draghi, M., Pashine, A., Sanjanwala, B., Gendzekhadze, K., Cantoni, C., Cosman, D., *et al.* NKp46 and NKG2D recognition of infected dendritic cells is necessary for NK cell activation in the human response to influenza infection. *J Immunol* **178**, 2688–2698 (2007).

22. Osterburg, A. R., Lach, L., Panos, R. J. & Borchers, M. T. Unique natural killer cell subpopulations are associated with exacerbation risk in chronic obstructive pulmonary disease. *Scientific Reports* **10**, 1238 (2020).

23. Vitale, M., Caligiuri, M. A. & Sivori, S. Editorial: Natural Killer Cells in Tissue Compartments. *Frontiers in Immunology* **11**, 258 (2020).

24. Marquardt, N., Kekäläinen, E., Chen, P., Lourda, M., Wilson, J. N., Scharenberg, M., *et al.* Unique transcriptional and protein-expression signature in human lung tissue-resident NK cells. *Nature Communications* **10**, 1–12 (2019).

25. Scharenberg, M., Vangeti, S., Kekäläinen, E., Bergman, P., Al-Ameri, M., Johansson, N., *et al.* Influenza A Virus Infection Induces Hyperresponsiveness in Human Lung Tissue-Resident and Peripheral Blood NK Cells. *Frontiers in Immunology* **10**, 1116 (2019).

26. Donovan, C., Starkey, M. R., Kim, R. Y., Rana, B. M. J., Barlow, J. L., Jones, B., *et al.* Roles for T/B lymphocytes and ILC2s in experimental chronic obstructive pulmonary disease. *Journal of Leukocyte Biology* **105**, 143–150 (2019).

27. Jones, B., Donovan, C., Liu, G., Gomez, H. M., Chimankar, V., Harrison, C. L., *et al.* Animal models of COPD: What do they tell us? *Respirology* vol. 22 21–32 (2017).

28. Liu, G., Cooley, M. A., Jarnicki, A. G., Hsu, A. C.-Y., Nair, P. M., Haw, T. J., *et al.* Fibulin-1 regulates the pathogenesis of tissue remodeling in respiratory diseases. *JCI Insight* **1**, (2016).

29. Lu, Z., van Eeckhoutte, H., Liu, G., Nair, P., Jones, B., Gillis, C., *et al.* Necroptosis Signalling Promotes Inflammation, Airway Remodelling and Emphysema in COPD. *Am J Respir Crit Care Med* (2021) doi:10.1164/RCCM.202009-3442OC.

30. Skerrett-Byrne, D., Bromfield, E., Murray, H., Jamaluddin, M., Jarnicki, A., Fricker, M., *et al.* Time-resolved proteomic profiling of cigarette smoke-induced experimental chronic obstructive pulmonary disease. *Respirology* (2021) doi:10.1111/RESP.14111.

31. Fricker, M., Goggins, B., Mateer, S., Jones, B., Kim, R., Gellatly, *et al.* Chronic cigarette smoke exposure induces systemic hypoxia that drives intestinal dysfunction. *JCI Insight* **3**, (2018).

32. Kant, N., Müller, R., Braun, M., Gerber, A. & Groneberg, D. Particulate Matter in Second-Hand Smoke Emitted from Different Cigarette Sizes and Types of the Brand Vogue Mainly Smoked by Women. *International Journal of Environmental Research and Public Health* **13**, (2016).

33. Kim, R. Y., Horvat, J. C., Pinkerton, J. W., Starkey, M. R., Essilfie, A. T., Mayall, J. R., *et al.* MicroRNA-21 drives severe, steroid-insensitive experimental asthma by amplifying phosphoinositide 3-kinase–mediated suppression of histone deacetylase 2. *Journal of Allergy and Clinical Immunology* **139**, 519–532 (2017).

34. Chen-Yu Hsu, A., Starkey, M. R., Hanish, I., Parsons, K., Haw, T. J., Howland, L. J., *et al.* Targeting PI3K-p110α Suppresses Influenza Virus Infection in Chronic Obstructive Pulmonary Disease. *American Journal of Respiratory and Critical Care Medicine* **191**, 1012–1023 (2015).

35. Hsu, A. C.-Y., Dua, K., Starkey, M. R., Haw, T.-J., Nair, P. M., Nichol, K., *et al.* MicroRNA-125a and -b inhibit A20 and MAVS to promote inflammation and impair antiviral response in COPD. *JCI Insight* **2**, (2017).

36. McKendry, R. T., Spalluto, C. M., Burke, H., Nicholas, B., Cellura, D., Al-Shamkhani, A., *et al.* Dysregulation of Antiviral Function of CD8(+) T Cells in the Chronic

Obstructive Pulmonary Disease Lung. Role of the PD-1–PD-L1 Axis. *Am J Respir Crit Care Med* **193**, 642–651 (2016).

37. Staples, K. J., Nicholas, B., McKendry, R. T., Spalluto, C. M., Wallington, J. C., Bragg, C. W., *et al.* Viral infection of human lung macrophages increases PDL1 expression via IFNbeta. *PLoS One* **10**, e0121527 (2015).

38. Nicholas, B., Staples, K. J., Moese, S., Meldrum, E., Ward, J., Dennison, P., *et al.* A novel lung explant model for the ex vivo study of efficacy and mechanisms of anti-influenza drugs. *J Immunol* **194**, 6144–6154 (2015).

39. Spits, H., Bernink, J. H. & Lanier, L. NK cells and type 1 innate lymphoid cells: partners in host defense. *Nat Immunol* **17**, 758–764 (2016).

40. Peng, H., Jiang, X., Chen, Y., Sojka, D. K., Wei, H., Gao, X., *et al.* Liver-resident NK cells confer adaptive immunity in skin-contact inflammation. *J Clin Invest* **123**, 1444–1456 (2013).

41. Valero-Pacheco, N. & Beaulieu, A. M. Transcriptional Regulation of Mouse Tissue-Resident Natural Killer Cell Development. *Frontiers in Immunology* vol. 11 309 (2020).

42. Ni, X., Fu, B., Zhang, J., Sun, R., Tian, Z. & Wei, H. Cytokine-based generation of CD49a+Eomes-/+ natural killer cell subsets. *Frontiers in Immunology* **9**, (2018).

43. Sojka, D. K., Plougastel-Douglas, B., Yang, L., Pak-Wittel, M. A., Artyomov, M. N., Ivanova, Y., *et al.* Tissue-resident natural killer (NK) cells are cell lineages distinct from thymic and conventional splenic NK cells. *Elife* **3**, e01659 (2014).

44. Xue, J., Schmidt, S. V, Sander, J., Draffehn, A., Krebs, W., Quester, I., *et al.* Transcriptome-based network analysis reveals a spectrum model of human macrophage activation. *Immunity* **40**, 274–288 (2014).

45. Wortham, B. W., Eppert, B. L., Motz, G. T., Flury, J. L., Orozco-Levi, M., Hoebe, K., *et al.* NKG2D Mediates NK Cell Hyperresponsiveness and Influenza-Induced Pathologies in a Mouse Model of Chronic Obstructive Pulmonary Disease. *The Journal of Immunology* **188**, 4468–4475 (2012).

46. Starkey, M. R., Jarnicki, A. G., Essilfie, A. T., Gellatly, S. L., Kim, R. Y., Brown, A. C., *et al.* Murine models of infectious exacerbations of airway inflammation. *Current Opinion in Pharmacology* **13**, 337–344 (2013).

47. Kurai, D., Saraya, T., Ishii, H. & Takizawa, H. Virus-induced exacerbations in asthma and COPD. *Frontiers in Microbiology* vol. 4 293 (2013).

48. De Serres, G., Lampron, N., La Forge, J., Rouleau, I., Bourbeau, J., Weiss, K., *et al.* Importance of viral and bacterial infections in chronic obstructive pulmonary disease exacerbations. *Journal of Clinical Virology* **46**, 129–133 (2009).

49. Dimopoulos, G., Lerikou, M., Tsiodras, S., Chranioti, A., Perros, E., Anagnostopoulou, U., *et al.* Viral epidemiology of acute exacerbations of chronic obstructive pulmonary disease. *Pulmonary Pharmacology and Therapeutics* **25**, 12–18 (2012).

50. Bekkat-Berkani, R., Wilkinson, T., Buchy, P., Dos Santos, G., Stefanidis, D., Devaster, J.-M., *et al.* Seasonal influenza vaccination in patients with COPD: a systematic literature review. *BMC Pulm Med* **17**, 79 (2017).

Competing interests: KS and TW have applied for a patent for the explant infection model (PCT/GB2010/050821 "*Ex Vivo* Modelling of Therapeutic Interventions"). They report funding from GSK Biologicals SA and AstraZeneca outside of the submitted work. TM reports grants,

personal fees from GlaxoSmithKline, outside the submitted work and is shareholder from Oryzon Genomics and Mendelion Lifesciences SL and holds a Chiesi chair on Environmental factors in Asthma. PH report funding from Aus-Bio, Allakos, Pharmakea, Astrazeneca, Genentec, Ionis, Glycosinovations, RAGE therapeutics, NextScience, Cincera, Lateral Pharma, MucPharma and Gertrude Biomedical outside of the submitted work. GC, JM, CD, TH, KB, NH, EB, CK and SK have no potential conflict of interest to declare.

Figures:

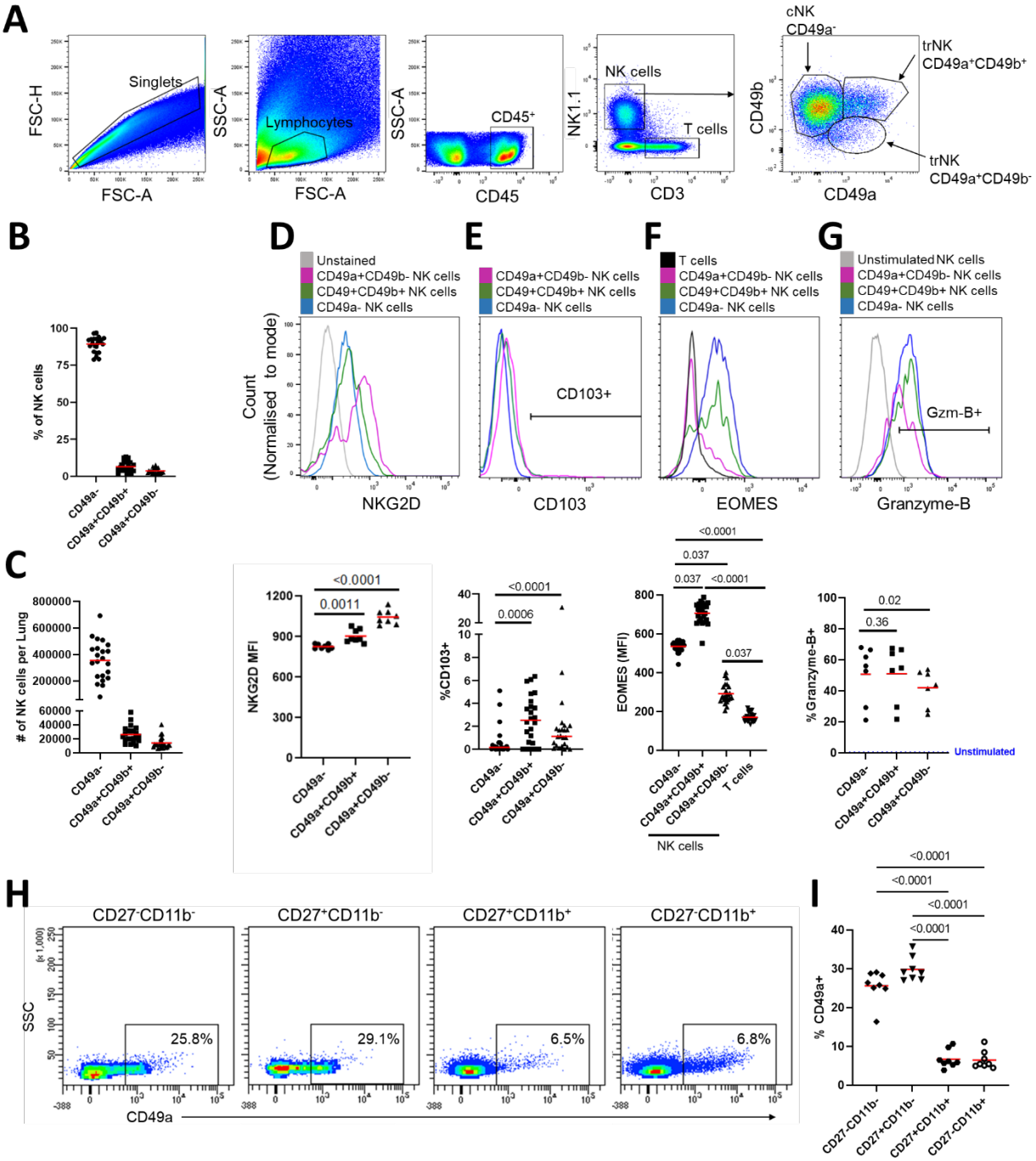

Fig. 1: Identification and characterization of CD49a^{+}CD49b^{-} trNK cells in murine lungs. (A) Gating strategy to define murine lung trNK cells. CD49a and CD49b expression on CD45^{+}CD3^{-}

591 NK1.1^{+} cells was determined based on Fluorescence-Minus-One (FMO) controls (Fig. E2A). (B,
592 C) Quantification of CD49a^{-}CD49b^{var}, CD49a^{+}CD49b^{+} and CD49a^{+}CD49b^{-} NK cells in murine
593 lungs, as a proportion of the whole NK cell population (CD45^{+}CD3^{-}NK1.1^{+} cells, B) and total
594 numbers per lung (C). (D-G) Representative flow cytometry plots and quantitation of CD49a^{-}
595 CD49b^{var} (blue; circle), CD49a^{+}CD49b^{+} (green; square) and CD49a^{+}CD49b^{-} (pink; triangle) NK
596 cell expression of NKG2D (D; N=8), CD103 (E; N=24), EOMES (F; N=24), and granzyme-B (G;
597 N=8). (H) Representative flow cytometry plots and (I) quantitation of CD49a expression in CD27^{-}
598 CD11b^{-}, CD27^{+}CD11b^{-}, CD27^{+}CD11b^{+}, and CD27^{-}CD11b^{+} NK cells (CD45^{+}CD3^{-}NK1.1^{+} cells;
599 N=8). (B, C, F) Cumulative results from three independent experiments are shown, for all other
600 panels data from a single experiment is reported. Lines describe means. Statistical analysis by
601 paired two-tailed t-test (B-E, G), one-way ANOVA with Bonferroni's multiple comparison
602 correction (I) or repeated measures one-way ANOVA with Bonferroni multiple comparison
603 correction (F).
604

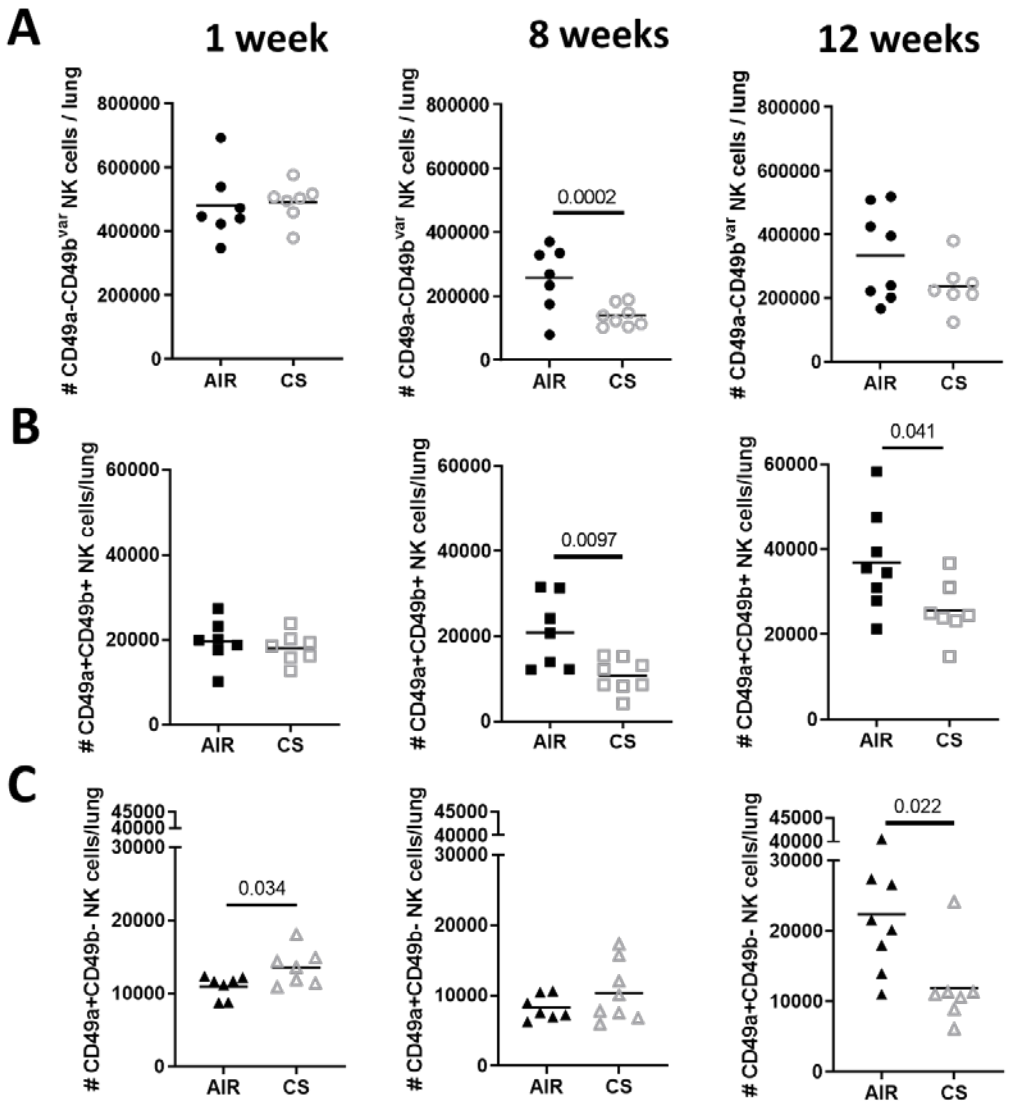

Fig. 2: CS exposure alters the numbers of CD49a$^+$ NK cells in the murine lung. Numbers of (A) CD49a$^-$CD49b^{var}, (B) CD49a$^+$CD49b$^+$ and (C) CD49a$^+$CD49b$^-$ NK cells per lung in normal air or CS exposed mice after 1, 8 or 12 weeks (N=7-8 per group). Horizontal lines show means. Statistical analysis by unpaired t-test. Data is from a single experiment and experimental time points were assayed separately.

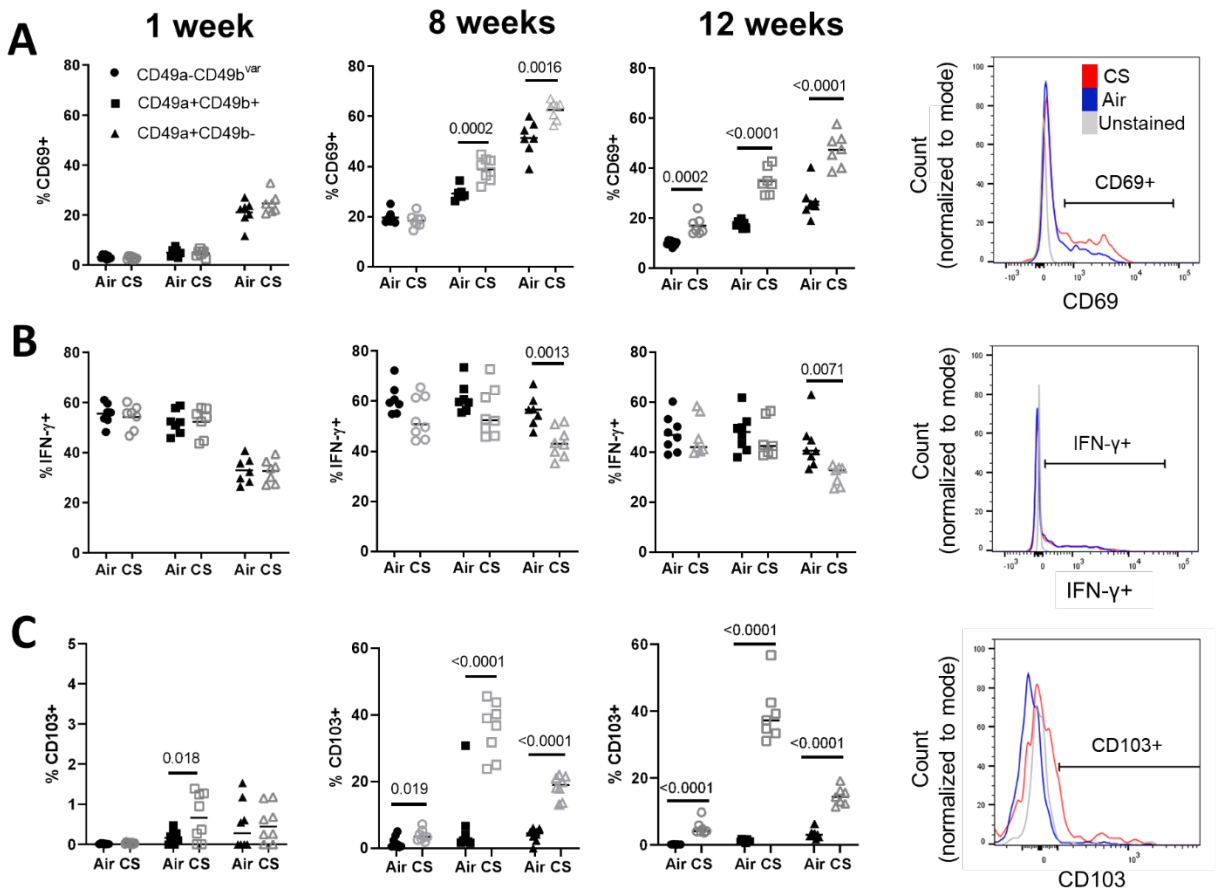

Fig. 3: CS exposure and experimental COPD are associated with altered NK cell functionality. Proportion of murine lung $CD49a^{-}CD49b^{var}$, $CD49a^{+}CD49b^{+}$ and $CD49a^{+}CD49b^{-}$ NK cells expressing (A) CD69, (B) IFN-γ and (C) CD103 in normal air or CS exposed mice after 1, 8 or 12 weeks. $CD49a^{-}CD49b^{var}$ NK (circles), $CD49a^{+}CD49b^{+}$ NK (squares) and $CD49a^{+}CD49b^{-}$ (triangles) cells and air- (closed symbols) and CS-exposed (open symbols) mice are indicated. Horizontal lines show means. Data is from a single experiment. Statistical analysis by unpaired t-test. Representative flow cytometry plots show gating on whole NK cell populations.

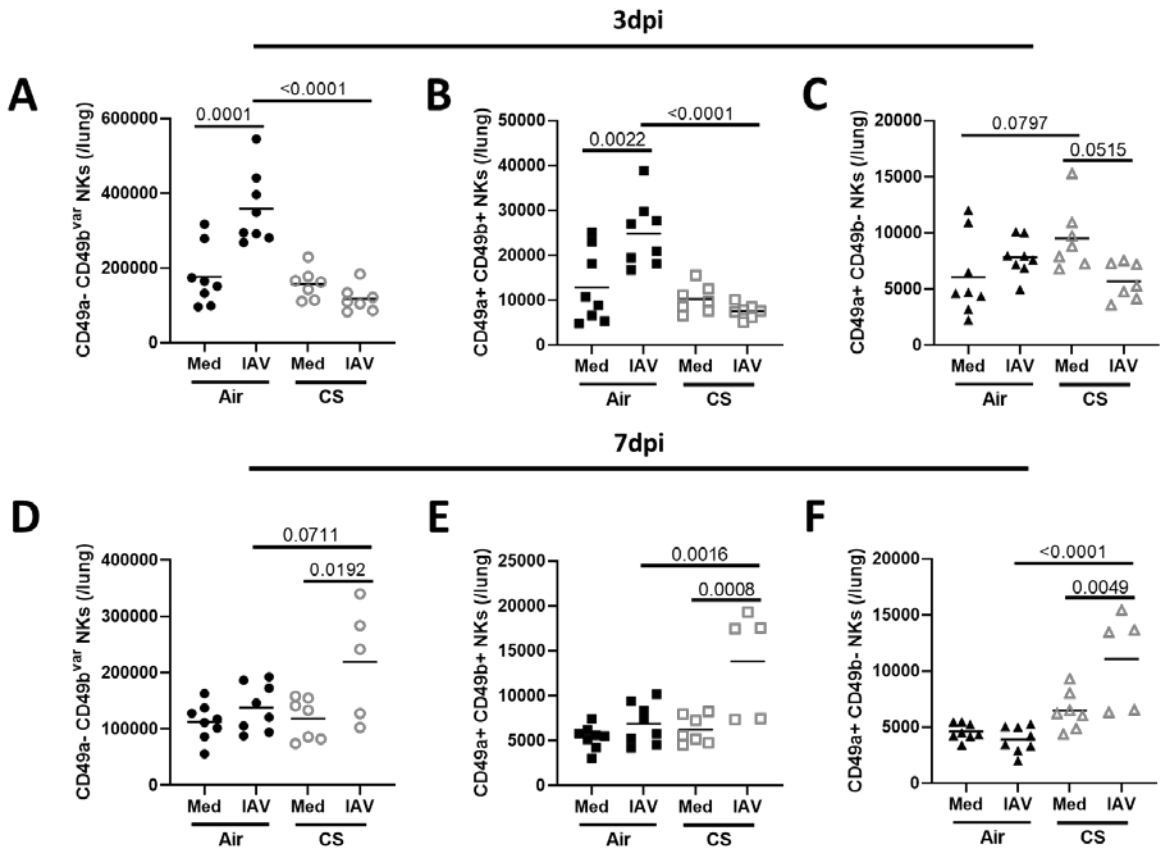

622

623 **Fig. 4: Chronic CS exposure delays the responses of cNK and trNK cells to IAV infection.**
624 Numbers of (A, D) $CD49a^{-}CD49b^{var}$, (B, E) $CD49a^{+}CD49b^{+}$ and (C, F) $CD49a^{+}CD49b^{-}$ NK cells
625 per lung in normal air- or CS-exposed mice after 10 weeks followed by IAV (H1N1 A/PR/8) or
626 mock (Med, media) infection for (A-C) 3 or (D-F) 7 days. Horizontal lines show means. Data is
627 from a single experiment. Statistical analysis by one-way ANOVA with Bonferroni's multiple
628 comparison correction (N=5-8/group).

629

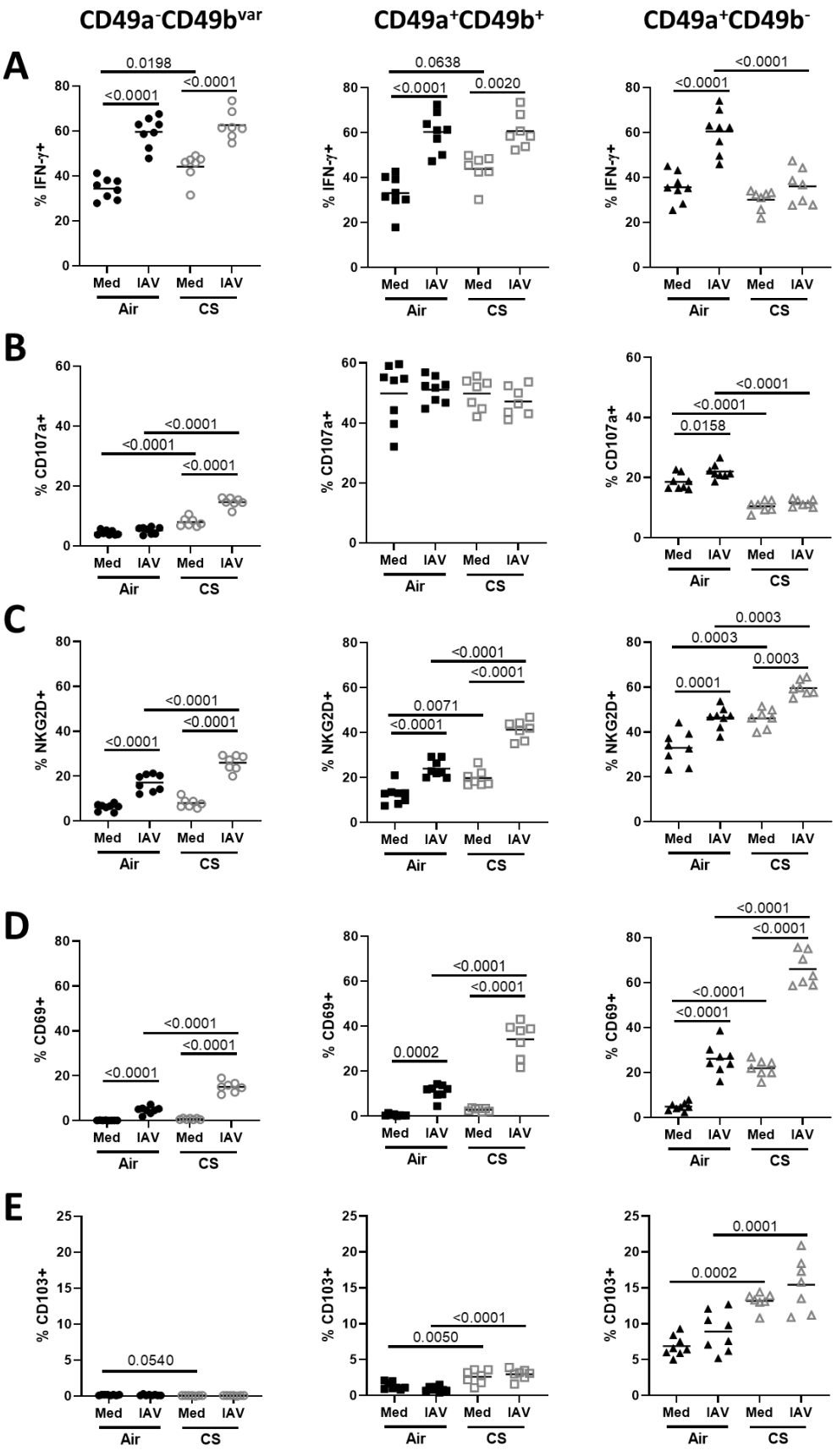
CD49a-CD49bvar
CD49a+CD49b+
CD49a+CD49b-
A
% IFN-γ+
0.0198
<0.0001
<0.0001
0.0638
<0.0001
0.0020
<0.0001
<0.0001
B
% CD107a+
<0.0001
<0.0001
<0.0001
<0.0001
<0.0001
0.0158
C
% NKG2D+
<0.0001
<0.0001
<0.0001
<0.0001
0.0071
<0.0001
0.0003
0.0003
0.0003
0.0001
D
% CD69+
<0.0001
<0.0001
<0.0001
<0.0001
0.0002
<0.0001
<0.0001
<0.0001
<0.0001
<0.0001
E
% CD103+
0.0540
<0.0001
0.0050
0.0001
0.0002
Med
IAV
Med
IAV
Air
CS

630

Fig. 5: Chronic CS exposure dysregulates the functional responses of cNK and trNK cells to IAV. Proportion of murine lung $CD49a^{-}CD49b^{var}$, $CD49a^{+}CD49b^{+}$ and $CD49a^{+}CD49b^{-}$ NK cells expressing (A) IFN-γ, (B) CD107a, (C) NKG2D, (D) CD69 and (E) CD103 in normal air- or CS-exposed mice after 10 weeks followed by infection with IAV (H1N1 A/PR/8) or mock (Med, media) infection for 3 days (N=7-8/group). $CD49a^{-}CD49b^{var}$ (circles), $CD49a^{+}CD49b^{+}$ (squares) and $CD49a^{+}CD49b^{-}$ (triangles) NK cells and air- (closed symbols) and CS-exposed mice (open symbols) are indicated. Lines show means. Data is from a single experiment. Statistical analysis by one-way ANOVA with Bonferroni's multiple comparison correction.

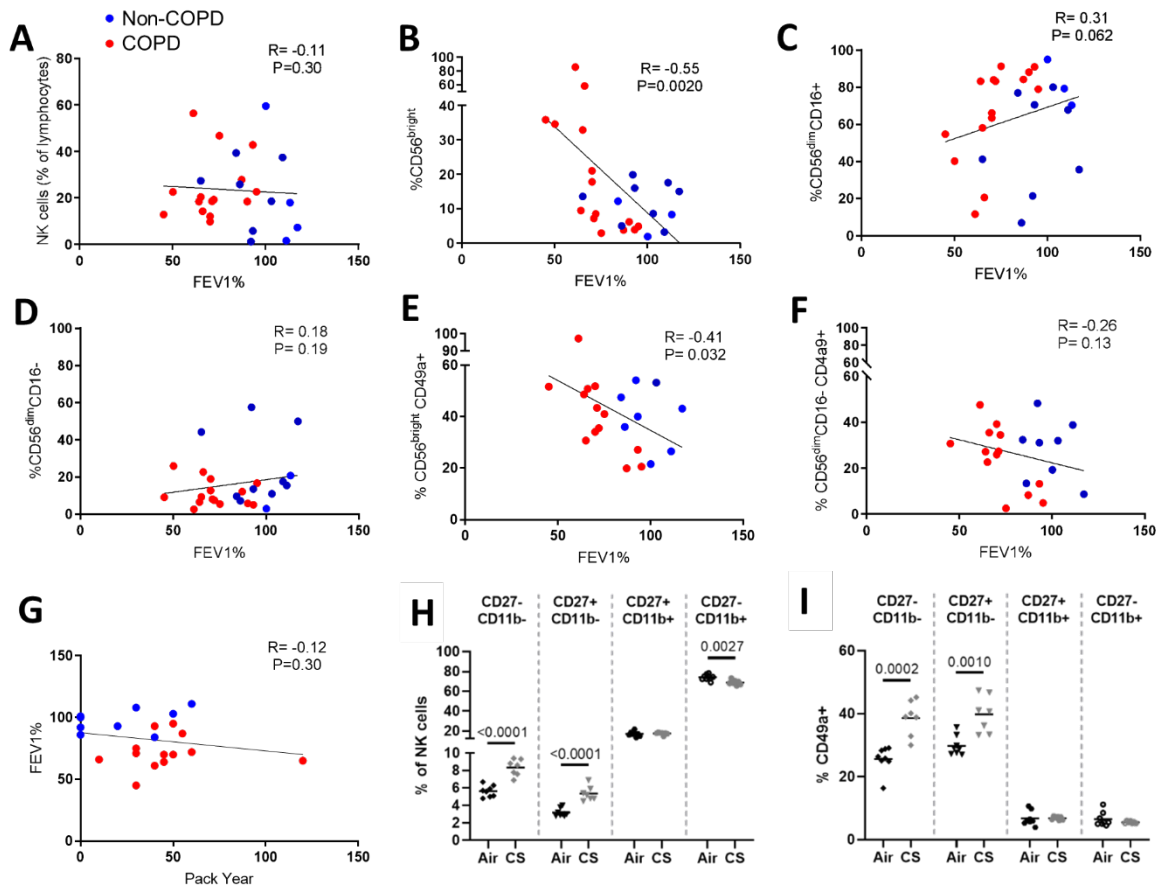

640

641 **Fig. 6: NK cell phenotypic features correlate with FEV$_1$% in humans and equivalent**
642 **phenotypic shifts are observed in experimental COPD.** Frequencies of (A) total NK cells (CD3$^-$
643 CD56$^+$ cells; as a proportion of CD45$^+$ lymphocytes), (B) CD56^{bright}, (C) CD56^{dim}CD16$^+$ and (D)
644 CD56^{dim}CD16$^-$ NK cells (as a proportion of total NK cells), and (E) CD56^{bright}CD49a$^+$ and (F)
645 CD56^{dim}CD16$^-$CD49a$^+$ NK cell subsets (as a proportion of CD56^{bright} or CD56^{dim}CD16$^-$ NK cells
646 respectively) in lung tissue from a mixed cohort of COPD (N= 17, red dots) and non-COPD
647 (N=15, blue dots) donors correlated with donor FEV$_1$%. (G) Pack year history correlated with
648 FEV1% for COPD and non-COPD human donors is shown. Pearson correlation co-efficient and
649 statistical analyses are shown. (H) Frequencies of CD27$^-$CD11b$^-$, CD27$^+$CD11b$^-$, CD27$^+$CD11b$^+$,
650 and CD27$^-$CD11b$^+$ NK cells as a proportion of CD45$^+$CD3$^-$NK1.1$^+$ NK cells and (I) frequency of

CD49a expression on $CD27^{-}CD11b^{-}$, $CD27^{+}CD11b^{-}$, $CD27^{+}CD11b^{+}$, and $CD27^{-}CD11b^{+}$ NK cells in lungs from normal air- or CS-exposed mice after 10 weeks. Horizontal lines show means. Data is from a single experiment. Statistical analysis by one-way ANOVA with Bonferroni's multiple comparison correction (N=7-8/group).

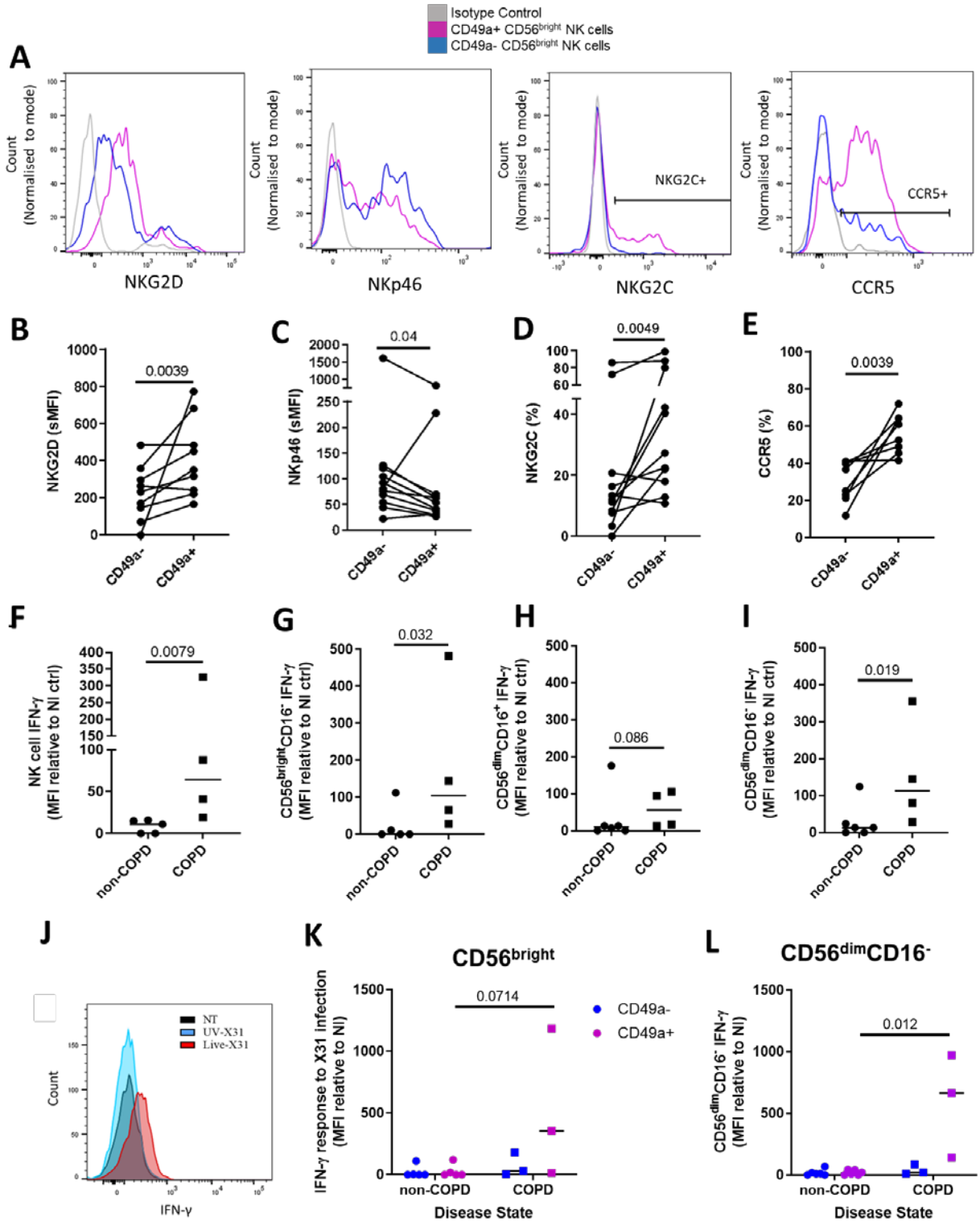

655

656 **Fig. 7: CD49a^{+} NK cells are phenotypically distinct from CD49a^{-} NK cells in the human lung.**

657 (A) Representative flow cytometry plots comparing the expression of NKp46, NKG2D, NKG2C

and CCR5 on CD49a^{+}CD56^{bright} and CD49a^{-}CD56^{bright} NK cells from human lung tissue. Quantification of marker expression for (B) NKG2D (N=10), (C) NKp46 (N=10), (D) NKG2C (N=11) and (E) CCR5 (N=8) on CD49a^{+}CD56^{bright} and CD49a^{-}CD56^{bright} lung NK cells. COPD and non-COPD donors are shown. For constitutively expressed proteins such as NKp46 and NKG2D, population MFI is reported. Statistical analysis by Wilcoxon signed-rank test. (F-I) NK cell intracellular IFN-γ accumulation after IAV infection in lung tissue explants from donors with and without a COPD diagnosis (COPD N=4, non-COPD N=6). Background fluorescence from non-infected (NI) tissue was subtracted from all values. IFN-γ production in (G) CD56^{bright}CD16^{-}, (H) CD56^{dim}CD16^{+} and (I) CD56^{dim}CD16^{-} NK cells is shown. (J) Representative flow cytometry plot of CD56^{bright} IFN-γ production in IAV-infected COPD lung tissue. IFN-γ production was compared between CD49a^{+} (purple dots) and CD49a^{-} populations (blue dots) of (K) CD56^{bright} and (L) CD56^{dim}CD16^{-} NK cells in COPD and non-COPD lung. Lines describe medians, statistical analysis was performed by Mann-Whitney test.

672 **Online Data Supplement**

673 **Anti-viral responses of tissue-resident CD49a^{+} lung NK cells are dysregulated in COPD**

674 Grace E. Cooper[1]†, Jemma Mayall[2]†, Chantal Donovan[2,3], Tatt J. Haw[2], Kurtis F. Budden[2], Nicole

675 G. Hansbro[3], Evy E. Blomme[4], Tania Maes[4], Chia Wei Kong[1], Jay C. Horvat[2], Salim I. Khakoo[1],

676 Tom M.A. Wilkinson[1,5,6], Philip M. Hansbro[2,3]†*, Karl J. Staples[1,5,6]†*

677

Supplementary Information

Supplementary Methods

Study Design. We aimed to characterize the phenotypes of lung trNK cells compared to cNK cells and examine the effects of CS exposure and COPD development on the phenotype and function of these cells. To do this controlled laboratory experiments were performed in both a murine model and human clinical samples. For the CS-induced experimental COPD model, mice were randomly assigned to groups and groups of 5-8 mice were used. For the characterization of trNK cell populations in naïve mice, up to 8 mice were used per individual experiment. Group sizes were not altered throughout the course of the study. Power calculations were not used to determine sample size, which were based on extensive experience. Groups that are compared were collected and processed at the same time. Outlier testing (Grubbs) was performed on all datasets and statistical outliers removed. For animal data, parametric analyses were used and mean summarized. Experiments were repeated at different timepoints of CS exposure and with/without IAV infection challenge. The analysis of the effect of CS exposure after three different lengths of time (1, 8 and 12 weeks) were performed independently with matched air controls in each experiment. Investigators were blinded for quantification of emphysematous changes but were not blinded for flow cytometric analyses. Human lung tissue and blood was collected opportunistically from cancer resection surgeries taking place at Southampton General Hospital. Analysis of human tissues was performed blinded with COPD status unknown to the researcher until the end of the study. Donors with known chronic lung infections were subsequently excluded from study (i.e tuberculosis). All patients assigned into the COPD subgroup had an established diagnosis of COPD or obstructive pattern spirometry with clinical or radiological evidence of COPD. Several patients assigned into the non-COPD subgroup had a FEV1/FVC ratio < 0.70 (mild degree). One non-

COPD donor had a diagnosis of asthma with no previous smoking exposure. All patients in the non-COPD subgroup have FEV1 and FVC values in the normal range or higher than predicted values, with no other clinical or radiological suspicion of COPD. For human datasets, non-parametric analyses were used and medians are shown due to data distribution.

Mice. All murine experiments were approved by the University of Newcastle Animal Care and Ethics Committee and performed at the Hunter Medical Research Institute, NSW, Australia. Eight-12 week-old female C57BL/6 mice were used as female mice are more susceptible to CS-induced airways remodeling and inflammatory factor upregulation, which reflects the increased risk of COPD seen in women compared to men, when amount of smoking is controlled [E1].

Murine immune cell isolation and stimulation. Lungs were digested with 2mg/mL collagenase D with 40U/mL DNase (Roche) in 5mL HEPES buffer (10mM HEPES-NaOH [pH7.4], 150mM NaCl, 5mM KCI, 1mM $MgCl_2$, 1.8mM $CaCl_2$) at 37°C for 30min with agitation and homogenised with a gentleMACS (Miltenyi) homogeniser. Red blood cells were removed with lysis buffer (155mM NH_4Cl, 12mM $NaHCO_3$, 0.1mM ethylenediaminetetraacetic acid [EDTA], pH 7.35) and the digest stimulated with 50ng/mL PMA and 1µg/mL ionomycin with 5µg/mL of brefeldin A (Sigma) for 5h.

Emphysema. Mouse lungs were perfused with 0.9% saline and inflated with (0.5mL) and submerged in 10% buffered formalin at the endpoint. Isovolumetric inflation was used in order to maintain lung architecture and avoid over-inflation which artificially increases alveolar size in mice with emphysema [E2]. Four µm thick sections of paraffin-embedded lung tissue were

mounted on microscope slides and stained with haematoxylin and eosin. A standardized template of horizontal lines was laid over randomly acquired micrographs (40x) of parenchymal tissue in lung sections (10 per mouse). The number of intercepts between alveolar walls and template lines were counted, the average number of intercepts for each mouse determined and MLI calculated based on cumulative length of template lines. Reduced numbers of intercepts and increased MLI length are an indicator of increased alveolar size and emphysema [E3,4].

Human tissue donors. This study was approved by Southampton and South West Hampshire Research Ethics Committee, UK 09/H0504/109, and all participants provided informed written consent. Seventeen out of the 32 tissue donors either had a pre-existing COPD diagnosis or were retrospectively diagnosed based on a reduced FEV_1% and FEV_1/forced vital capacity ratio, consistent with a global initiative for chronic obstructive lung disease (GOLD) diagnosis [E5]. The remaining 15 were classified as non-COPD. COPD and non-COPD donors were well matched for characteristics including age (P=0.39), gender (P=0.29), smoking status (P=0.4) and resection location (P=0.32, Table S1). COPD donors had a greater history of smoking with higher pack-years (median COPD; 45, non-COPD; 20; P=0.028) and inhaled corticosteroid use (in 10 out of 17 COPD donors; Table S1). Donors with known chronic lung infections were subsequently excluded from study (i.e tuberculosis).

Preparation of human lung tissue and explant infection. Lung tissue explants were cut into 4-6 mm^2 pieces with 6 fragments/well and washed with cold RPMI. Lung explants were rested for 16h in complete RPMI (RPMI with 10% FCS, 2 mg/mL L-glutamine, 0.05 IU/mL penicillin, 50 µg/mL streptomycin and 0. 25µg/mL amphotericin B, Sigma). Lung tissue was then digested in 0.5

mg/mL collagenase (37°C, 15min), passed through a 40 µm filter and centrifuged (800x*g*, 15min) over a Ficoll-paque layer. Cells isolated from the interface were stained for flow cytometry. Alternatively, for IAV infection of lung explants, lung fragments were infected with $3.15x10^7$ IU/mL live or UV-irradiated IAV following 16h rest [E6]. UV-irradiated IAV was created by exposing live virus to UV light for 2h on ice. Two-h post-infection, extracellular virus was removed by washing with PBS and explants cultured in fresh media for a further 14h. To measure intracellular cytokines, explants were then incubated with 2µM Monensin (eBioscience) for 24h. After infection, cells were dispersed from tissue by agitation in 0.5 mg/ml collagenase. Digests were filtered and cells stained for flow cytometry. Cells were resuspended in 100µL PBS and incubated with a 1:100 dilution of Zombie-Violet (Biolegend, San Diego, USA) amine binding dye for 30 min on ice.

Flow cytometry. All steps were performed in PBS containing 2mM EDTA and 1% BSA on ice unless otherwise stated. Cells were washed and incubated with 2mg/mL Fc block for 15min then incubated with fluorophore-conjugated antibodies against surface markers (Table S2) for 30min. Biotin-conjugated antibodies were subsequently labeled with fluorophore-conjugated streptavidin. Cells were fixed with 2% paraformaldehyde or Cytofix/Cytoperm (BD Biosciences). For intracellular staining, cells were incubated with antibodies in permeabilisation buffer (BD) for 30min. Data was acquired with a FACS Aria III or II and analysed with FACSDiva (BD) or FlowJo (TreeStar) software. The use of MFI or % was decided based on the histogram profile of the fluorescence readout of each marker. Where a distinct peak was observed relative to the unstained or FMO control then the % of population was reported (e.g CD103 and granzyme-B – Fig1&2),

but where a shift in the whole population was observed (e.g EOMES and NKG2D Fig1) then MFI was used

Fig. E1 – CS exposure induces alveolar enlargement in a mouse model of COPD and IAV infection has no additional affect.

Fig. E2: Quantification of $CD49a^+$ NK cells in the murine lung

Fig. E3: Proportions of $CD49a^+$ NK cells in the lungs of air- and CS-exposed mice over time

Fig. E4: Altered expression of functional and phenotypic markers on CD49a+ NK cell in CS-treated mice expressed as fold change relative to air controls.

Fig. E5: Proportions of $CD49a^-$, $CD49a^+CD49b^-$ and $CD49a^+CD49b^+$ NK cells in the lungs of air- and CS-exposed mice.

Fig. E6: Functional marker expression on $CD49a^+$ and $CD49a^-$ NK cells 7 dpi with IAV

Fig. E7: Gating strategy to define human $CD49a^+$ and $CD49a^-$ lung NK cells

Fig. E8: COPD severity, but not inhaled corticosteroid use or smoking status, is associated with altered human NK cell subpopulations.

Fig. E9: Expression of CCR5 and activating receptors on $CD56^{dim}CD16^-$ NK cells

Fig. E10: Expression of NK cell activating receptors are not affected by COPD status in humans

Table E1: Clinical demographics for resected human lung tissue cohort

Table E2: Antibodies used for flow cytometry

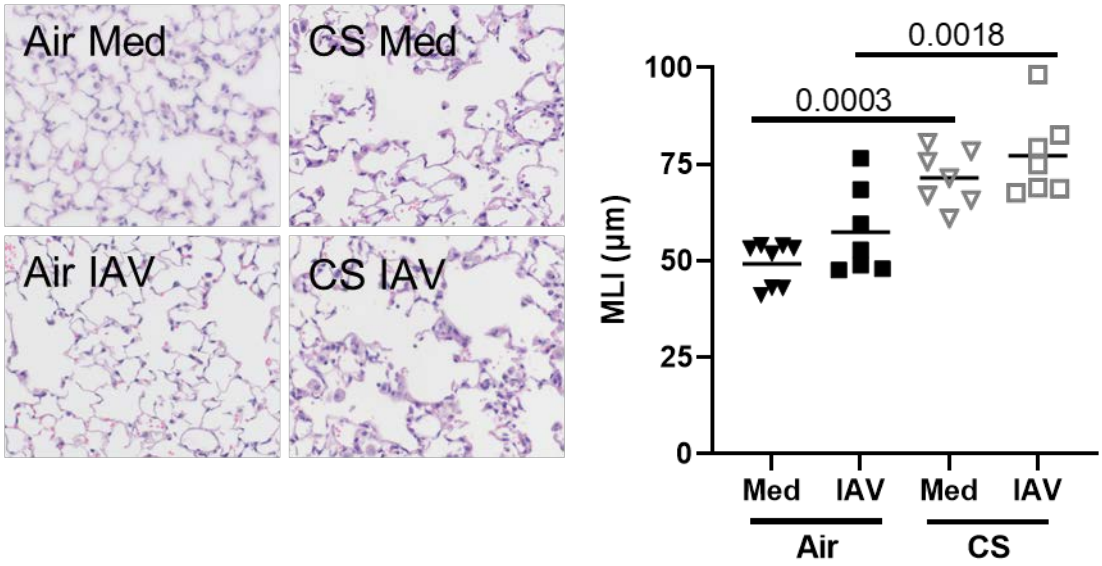

791

792 **Fig. E1 – CS exposure induces alveolar enlargement in a mouse model of COPD and IAV**
793 **infection has no additional affect.** Lungs were perfused and inflated and emphysema-like
794 alveolar enlargement assessed by determining alveolar wall mean linear intercept (MLI) in
795 haematoxylin and eosin stained sections from normal air- or CS-exposed mice after 10 weeks
796 followed by IAV (H1N1 A/PR/8) or mock (Med, media) infection for 3 days. Horizontal lines
797 show means. Statistical analysis by one-way ANOVA with Bonferroni's multiple comparison
798 correction (N=7-8/group).

799

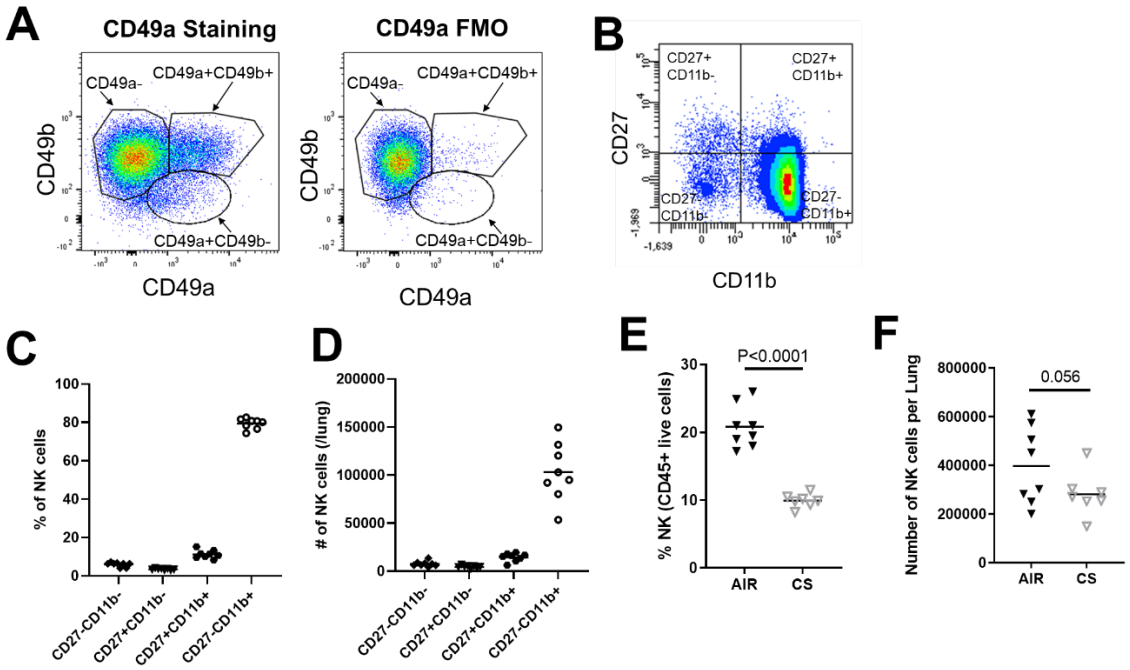

Fig. E2 - Quantification of CD49a+ NK cells in the murine lung. (A) Representative gating on CD49a+ NK cell populations in the mouse lung, gates were set from FMO controls after gating $CD45^{+}CD3^{-}NK1.1^{+}$ cells. (B) Gating strategy to define murine lung NK cell maturation state based on CD27 and CD11b expression. (C, D) Quantification of $CD27^{-}CD11b^{-}$, $CD27^{+}CD11b^{-}$, $CD27+CD11b^{+}$, and $CD27^{-}CD11b^{+}$ NK cells in murine lungs, as a proportion of NK cells and total numbers per lung. (E) Lung NK cells (defined as $CD3^{-}NK1.1^{+}$ cells) as a proportion of live lymphocytes ($CD45^{+}$) following 12 weeks of air or CS exposure. (F) Numbers of NK cells calculated per lung after 12 weeks of exposure. Cell number = Proportion of singlet gate x Total hemocytometer cell count. Lines describe mean. Statistical analysis by T-test (N=8).

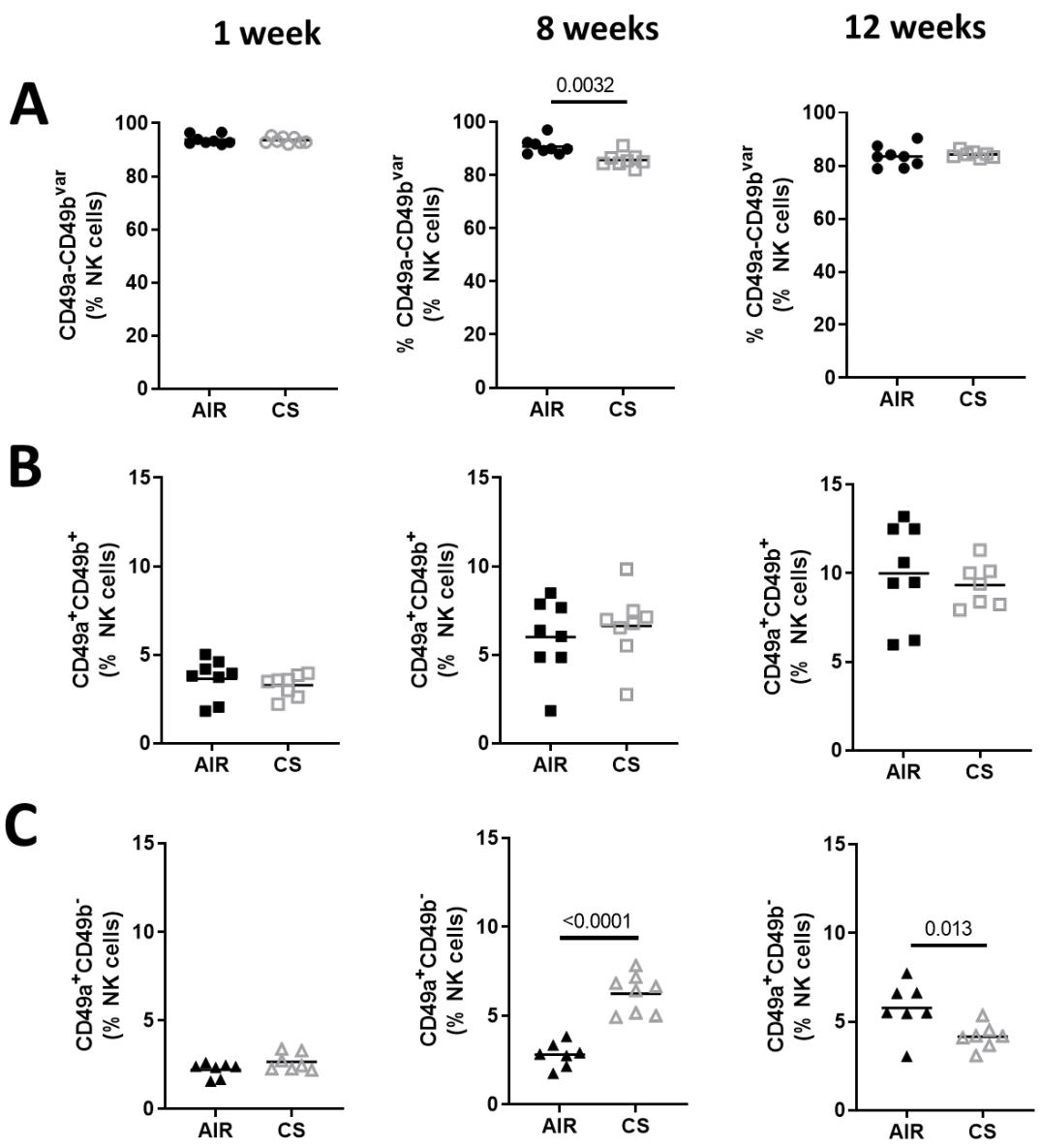

Fig. E3 - Proportions of CD49a+ NK cells in the lungs of air- and CS-exposed mice over time. The proportion of (A) $CD49a^{-}CD49b^{var}$, (B) $CD49a^{+}CD49b^{+}$ and (C) $CD49a^{+}CD46b^{-}$ within the NK cell population of mice exposed to air or CS for 1, 8 and 12 weeks of treatment. Horizontal lines show means. Statistical analysis was performed with a two-tailed unpaired T-test (7-8 mice / group).

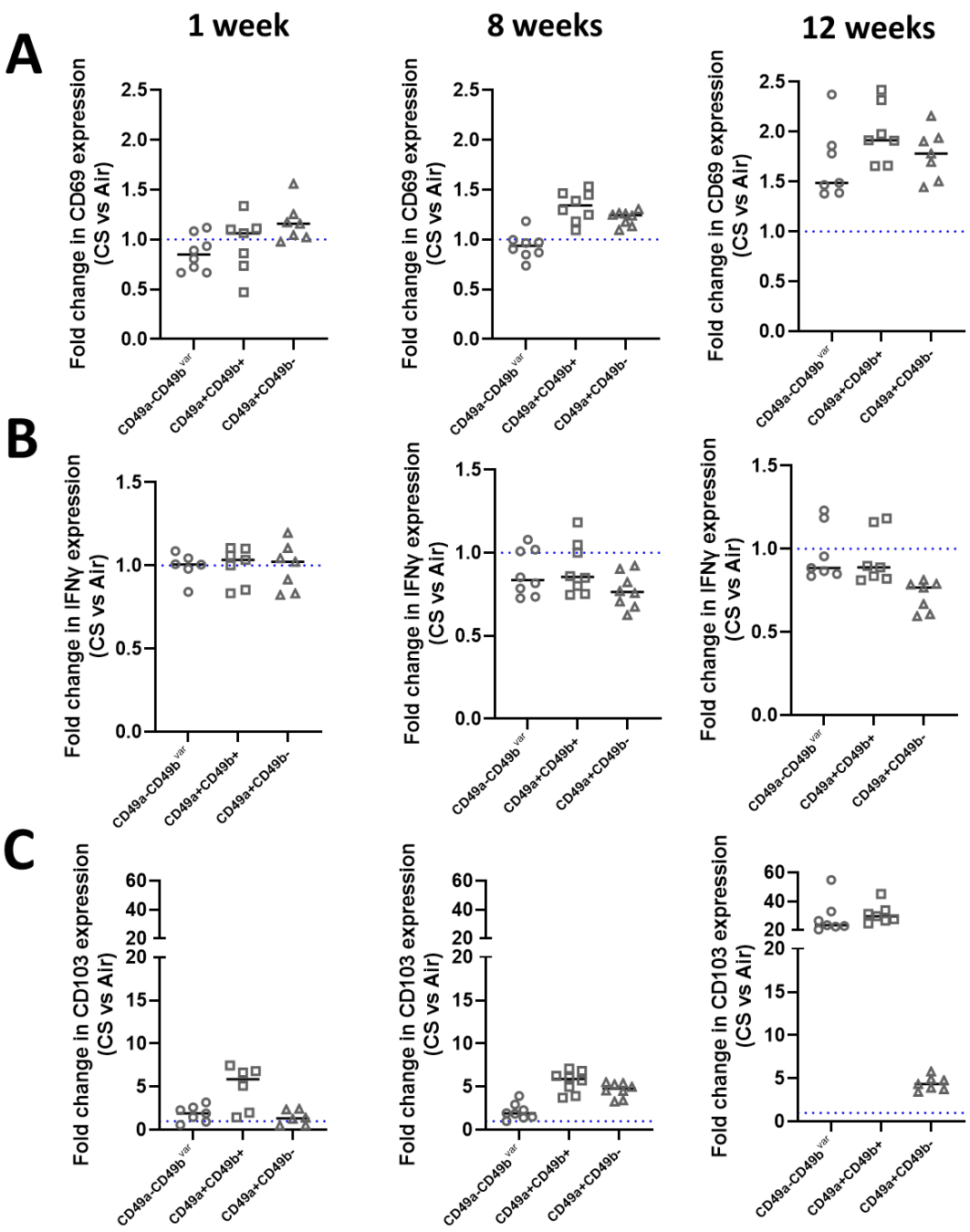

819

820

821 **Fig. E4 - Altered expression of functional and phenotypic markers on CD49a+ NK cell in**

822 **CS-treated mice expressed as fold change relative to air controls.** Blue dotted line represents

air treated controls. (A) % CD69 expression, (B) %IFN-γ expression and (C) % CD103 on CD49a+ and CD49a- NK cell subsets from the lung.

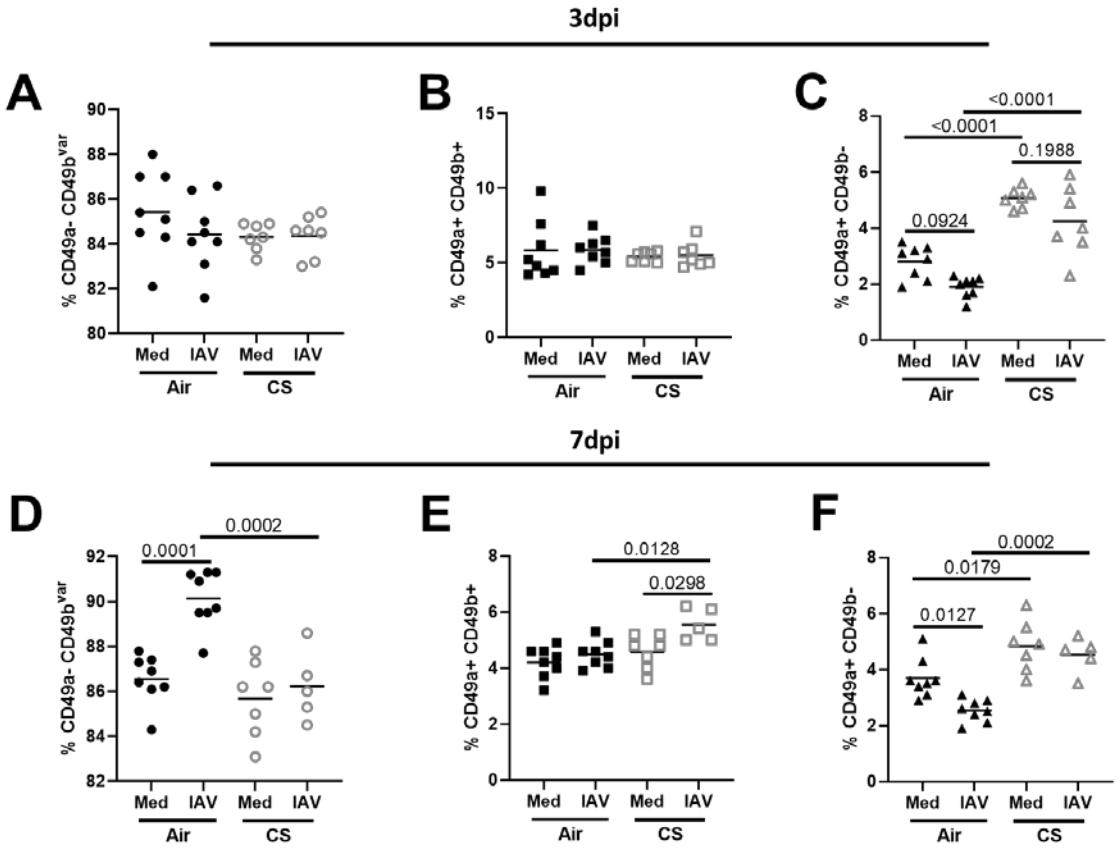

Fig. E5 - Proportions of CD49a$^-$, CD49a$^+$CD49b$^-$ and CD49a$^+$CD49b$^+$ NK cells in the lungs of air- and CS-exposed mice during IAV infection. The proportion of murine lung (A, D) CD49a-CD49bvar, (B, E) CD49a+CD49b+ and (C, F) CD49a+CD49b- NK cells in air or CS exposed mice after 10 weeks of exposure followed by infection with influenza A virus (IAV H1N1 A/PR/8) or mock (media) infection for (A, B, C) 3 or (D, E, F) 7 days. Lines show means. Statistical analysis by one way ANOVA with Bonferroni's multiple comparison correction.

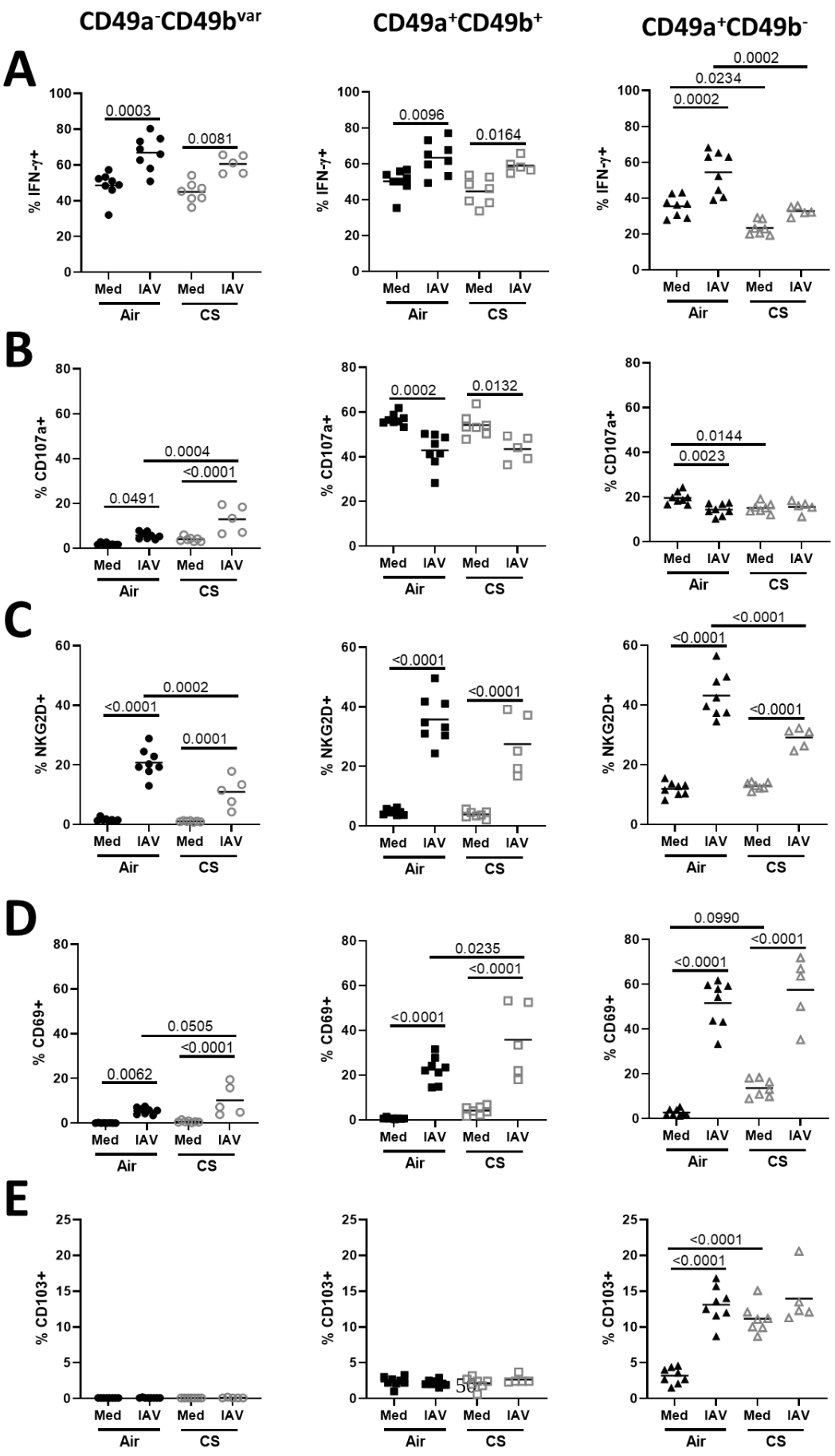
CD49a-CD49bvar
CD49a+CD49b+
CD49a+CD49b-
A
% IFN-γ+
0.0003
0.0081
0.0096
0.0164
0.0002
0.0234
0.0002
B
% CD107a+
0.0491
0.0004
<0.0001
0.0002
0.0132
0.0023
0.0144
C
% NKG2D+
<0.0001
0.0002
0.0001
<0.0001
<0.0001
<0.0001
<0.0001
D
% CD69+
0.0062
0.0505
<0.0001
<0.0001
0.0235
<0.0001
<0.0001
0.0990
<0.0001
E
% CD103+
<0.0001
<0.0001
Med
IAV
Air
CS

835

Fig. E6 - Functional marker expression on CD49a+ and CD49a- NK cells 7 dpi with IAV. The proportion of murine lung CD49a^{-}CD49b^{var}, CD49a^{+}CD49b^{+} and CD49a^{+}CD49b^{-} NK cells expressing (A) IFN-γ, (B) CD107a, (C) NKG2D, (D) CD69 and (E) CD103 in mice after 10 weeks of air or CS exposure followed by infection with IAV (H1N1 A/PR/8) or mock (media) infection for 7 days. CD49a^{-}CD49b^{var} NK cells (circles), CD49a^{+}CD49b^{+} NK cells (squares) and CD49a^{+}CD49b^{-} (triangles), air (closed symbols) and CS-exposure (open symbols) are shown. Horizontal lines show means. Statistical analysis using one way ANOVA with Bonferroni's multiple comparison correction.

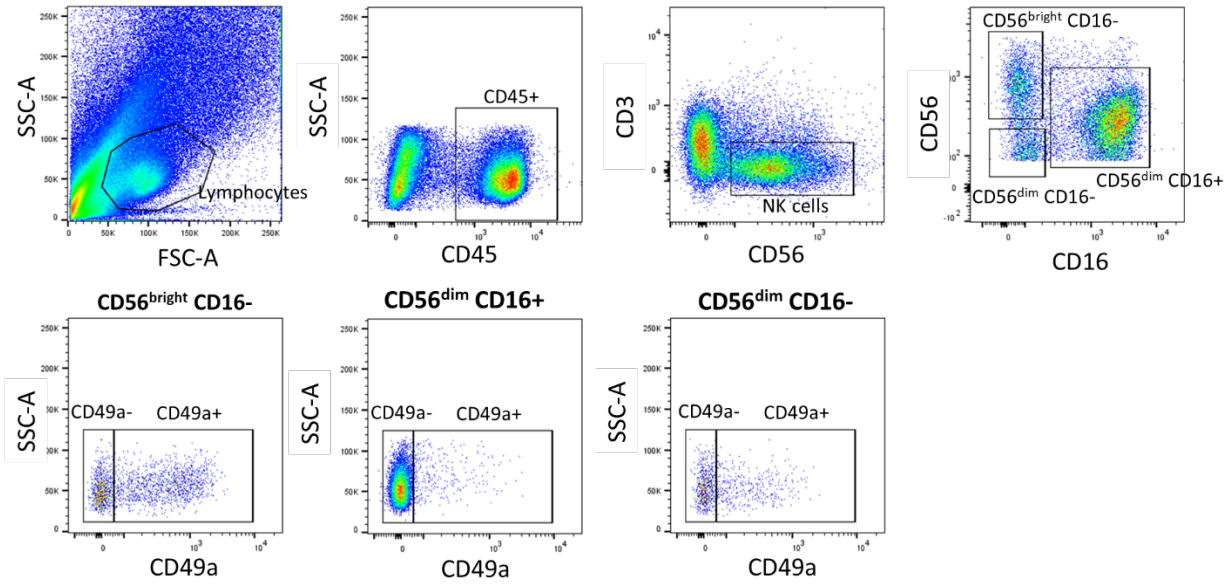

Fig. E7 - Gating strategy to define human CD49a^{+} and CD49a^{-} lung NK cells. NK cells were defined as CD45^{+}CD3^{-}CD56^{+} cells and further stratified into CD56^{bright}CD16^{-}, CD56^{dim}CD16^{+} and CD56^{dim}CD16^{-} NK cells.

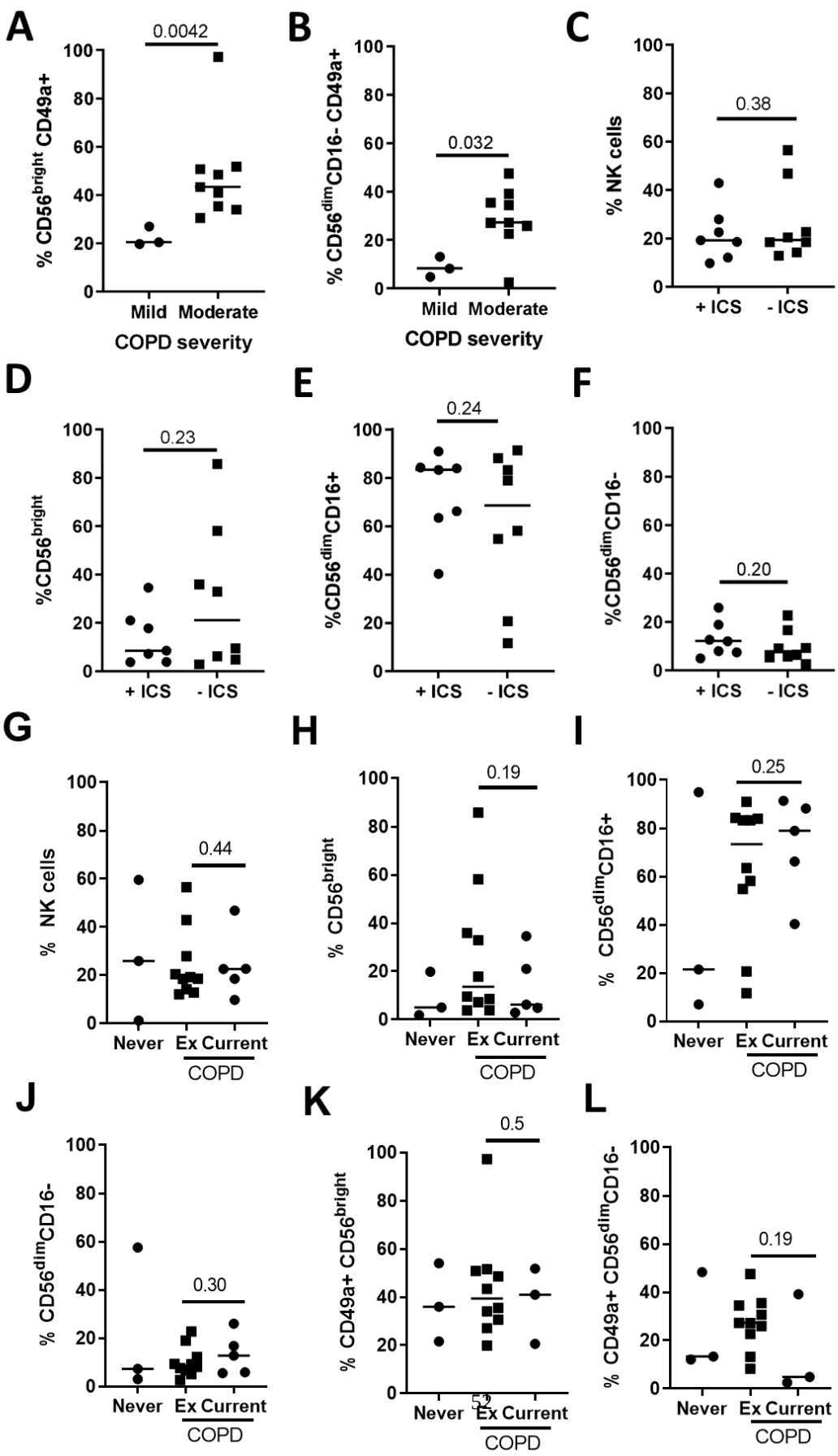
A
0.0042
% CD56bright CD49a+
Mild Moderate
COPD severity
B
0.032
% CD56dim CD16- CD49a+
Mild Moderate
COPD severity
C
0.38
% NK cells
+ ICS - ICS
D
0.23
%CD56bright
+ ICS - ICS
E
0.24
%CD56dim CD16+
+ ICS - ICS
F
0.20
%CD56dim CD16-
+ ICS - ICS
G
0.44
% NK cells
Never Ex Current
COPD
H
0.19
% CD56bright
Never Ex Current
COPD
I
0.25
% CD56dim CD16+
Never Ex Current
COPD
J
0.30
% CD56dim CD16-
Never Ex Current
COPD
K
0.5
% CD49a+ CD56bright
Never Ex Current
COPD
L
0.19
% CD49a+ CD56dim CD16-
Never Ex Current
COPD

851

Fig. E8 - COPD severity, but not inhaled corticosteriod use or smoking status, is associated with altered NK cell subpopulations in human lung. (A, B) Proportions of (A) $CD49a^{+}$ $CD56^{bright}$ and (B) $CD49a^{+}CD56^{dim}CD16^{-}$ cells within the NK cell population, stratified by mild and moderate COPD status as defined by GOLD guidelines (donors not using ICS N=7). (C) The proportion of NK cells as a percentage of $CD45^{+}$ lymphocytes in donors that were using ICS (N=7) *versus* those that were not (N=8). (D-F) Proportions of $CD56^{bright}$ and $CD56^{dim}CD16^{-}$ subsets within the whole NK cell population stratified by ICS use. (G) The proportion of NK cells as a percentage of $CD45^{+}$ lymphocytes in donors that were current (N=4) or ex-smokers (N=10). (H-J) Proportions of $CD56^{bright}$ $CD56^{dim}CD16^{+}$ and $CD56^{dim}CD16^{-}$ NK cell subsets in current and ex-smokers. (K, L) Proportions of $CD49a^{+}$ $CD56^{bright}$ (K) and $CD56^{dim}CD16^{-}$ (L) NK cells stratified based on smoking status. (Current smokers N=3, ex-smokers N=10). Statistical analysis by two-tailed Mann-Whitney U-test. Horizontal lines show medians.

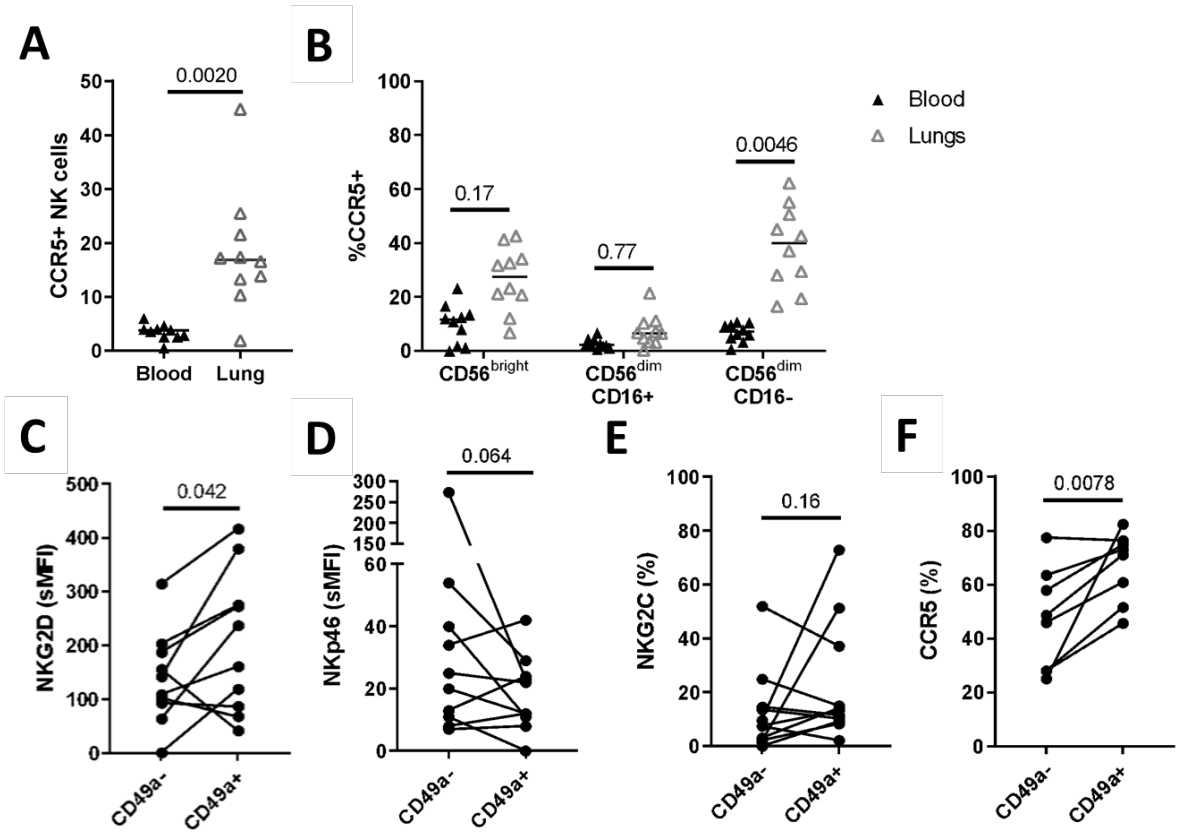

Fig. E9 - Expression of CCR5 and activating receptors on CD56^{dim}CD16^{-} NK cells in human lung and blood (A) CCR5 expression on NK cells isolated from human lungs and matched blood. (B) CCR5 expression on CD56^{bright} and CD56^{dim} NK cell subsets in human lung and matched blood. Horizontal lines show medians, statistical analysis used the Wilcoxon signed-rank test. (C-F) Quantification of surface marker expression of CD49a^{+} and CD49a^{-} CD56^{dim}CD16^{-} NK cells from human lung. NKG2D (C, N=10) NKp46 (D, N=10), NKG2C (E, N=11) and CCR5 (F, N=8) are reported. Horizontal lines show medians, statistical analysis used the Wilcoxon signed-rank test.

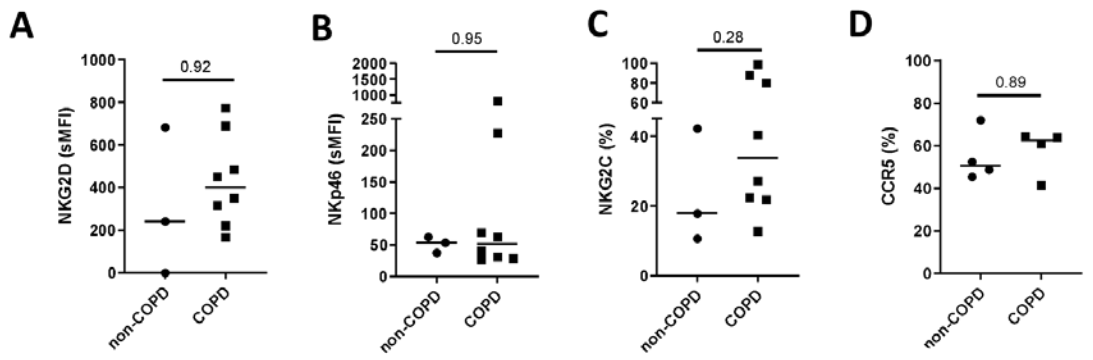

Fig. E10 - Expression of NK cell activating receptors are not affected by COPD status in humans. $CD49a^{+}CD56^{bright}$ NK cell expression of NKG2D (A), NKp46 (B), NKG2C (C) and CCR5 (D) in donors with and without COPD. Statistical analysis by Mann-Whitney test.

	COPD	Non-COPD	P value
Number of donors	17	15	
Age (median years)	70 (*8*)	76 (*14*)	0.39[1]
Gender (F / M)	9 / 8	11 / 4	0.29[2]
Smoking status (never / ex / current / unknown)	0 / 11 / 5 / 1	4 / 7 / 1 / 3	0.4[3]
Pack-years of smoking	45* *(20)*	20* *(35)*	0.028[1]
FEV1%	70 *(9.25)*	100.5 *(17.25)*	<0.001[1]
FEV1/FVC ratio	0.62 *(0.14)*	0.69 *(0.1)*	0.0026[1]
Resection Location (LUL/LLL/RUL/RML/RLL)	3 / 3 / 8 / 0 / 3	5 / 1 / 4 / 2 / 3	0.32[3]
Inhaled corticosteroid use (+/-)	10 / 7	0 / 15	0.0003[2]

Table S1: Clinical demographics for resected human lung tissue cohort. Median values are shown with italicized interquartile range values in brackets. Donor COPD status was obtained from formal diagnosis and low values in pulmonary function tests. Statistical analysis was performed with [1]Mann Whitney, [2]Fisher's two-sided or [3]Chi square tests. *Information not available for 4 donors.

888 **Table S2: Antibodies used for flow cytometry**

Target Species	Antigen	Fluorochrome	Cat #	Manufacturer	Clone
Mouse	CD45	PerCP	103130	Biolegend	30-F11
Mouse	CD3	APC	100311	Biolegend	145-2C11
Mouse	NK1.1	PE-Cy7	108714	Biolegend	PK136
Mouse	NKG2D	Biotin	115703	Biolegend	C7
Mouse	CD27	APC-Cy7	124225	Biolegend	LG.3A10
Mouse	CD11b	AF700	557960	BD	M1/70
Mouse	CD69	BUV395	740220	BD	H1.2F3
Mouse	CD107a	BV786	564349	BD	1D4B
Mouse	CD49b	PE-Dazzle594	108923	Biolegend	DX5
Mouse	CD49a	BV605	740375	BD	Ha31/8
Mouse	CD103	BUV737	749393	BD	2E7
Mouse	IFNγ	PE	505808	Biolegend	XMG1.2
Mouse	CD49b	FITC	108905	Biolegend	DX5
Mouse	CD49a	BV711	564863	BD	Ha31/8
Mouse	CD103	BV510	563087	BD	M290
Mouse	CD69	PECF594	562455	BD	H1.2F3
Mouse	GzmB	Biotin	13-8822-82	Thermo	16G6
Mouse	Eomes	eFluor450	48-4875-82	Thermo	Dan11mag
Human	CD45	BV510	563204	BD	HI30
Human	CD45	APC-Cy7	555485	BD	HI30

Human	CD3	PerCP	300428	Biolegend	UCHT1
Human	CD3	APC	300412	Biolegend	UCHT1
Human	CD56	PE-Cy7	318318	Biolegend	HCD56
Human	CD16	FITC	556618	BD	3G8
Human	CD49a	PE	559596	BD	SR84
Human	CCR5	PE-Dazzle594	359126	Biolegend	J418F1
Human	NKG2D	APC-Cy7	320824	Biolegend	1D11
Human	NKG2C	APC	FAB138A	R&D Systems	REA205
Human	NKp46	BV421	331914	Biolegend	9E2
Human	IFNγ	PerCP-Cy5.5	502526	Biolegend	4S.B3
	Streptavidin	BV421	405226	Biolegend	
	Streptavidin	BV650	405231	Biolegend	

Supplementary References

51. Tam, A., Churg, A., Wright, J. L., Zhou, S., Kirby, M., Coxson, H. O., *et al.* Sex Differences in Airway Remodeling in a Mouse Model of Chronic Obstructive Pulmonary Disease. *American Journal of Respiratory and Critical Care Medicine* **193**, 825–834 (2015).

52. Beckett, E. L., Stevens, R. L., Jarnicki, A. G., Kim, R. Y., Hanish, I., Hansbro, N. G., *et al.* A new short-term mouse model of chronic obstructive pulmonary disease identifies a role for mast cell tryptase in pathogenesis. *Journal of Allergy and Clinical Immunology* **131**, 752-762.e7 (2013).

103. Jarnicki, A. G., Schilter, H., Liu, G., Wheeldon, K., Essilfie, A. T., Foot, J. S., *et al.* The inhibitor of semicarbazide-sensitive amine oxidase, PXS-4728A, ameliorates key features of chronic obstructive pulmonary disease in a mouse model. *British Journal of Pharmacology* **173**, 3161–3175 (2016).

104. Liu, G., Cooley, M. A., Jarnicki, A. G., Hsu, A. C.-Y., Nair, P. M., Haw, T. J., *et al.* Fibulin-1 regulates the pathogenesis of tissue remodeling in respiratory diseases. *JCI Insight* **1**, (2016).

105. Vestbo, J., Hurd, S. S., Agustí, A. G., Jones, P. W., Vogelmeier, C., Anzueto, A., *et al.* Global strategy for the diagnosis, management, and prevention of chronic obstructive pulmonary disease GOLD executive summary. *American Journal of Respiratory and Critical Care Medicine* vol. 187 347–365 (2013).

106. Cooper, G. E., Ostridge, K., Khakoo, S. I., Wilkinson, T. M. A. & Staples, K. J. Human CD49a+ lung natural killer cell cytotoxicity in response to influenza A virus. *Frontiers in Immunology* **9**, 1671 (2018).